https://doi.org/10.5194/egusphere-2026-1342
Preprint. Discussion started: 18 March 2026

Paleoenvironmental and paleoclimatic reconstruction in the Western Mediterranean during the Late Early Pleistocene

Maé Catrain[1], Séverine Fauquette[2], Odile Peyron[2], Nathalie Combourieu-Nebout[1], Vincent Lebreton[1], Morgane Fischer-Fries[3], Mary Robles[2], Viviane Bout-Roumazeilles[4], Patricia Richard[3], Marion Delattre[4], Lionel Dubost[1], Sébastien Joannin[2], Yul Altolaguirre[5], Jean-Pierre Suc[6], Jeanne Lepelletier[1], Marie-Hélène Moncel[1]

[1] Histoire Naturelle des Humanités Préhistoriques, UMR 7194 HNHP, MNHN-CNRS-UPVD, Muséum National d'Histoire Naturelle, Paris, France

[2] ISEM, Univ. Montpellier, CNRS, IRD, EPHE, Montpellier, France

[3] Laboratoire des Sciences du Climat et de l'Environnement, UMR 8212 LSCE/IPSL, CEA-CNRS-UVSQ, Université Paris-Saclay, Gif-sur-Yvette, France

[4] Laboratoire d'Océanologie et de Géosciences, UMR 8187 LOG. CNRS, Université de Lille, Université du Littoral–Côte d'Opale, IRD, F-59000 Lille, France

[5] ROCEEH Research Centre 'The Role of Culture in Early Expansions of Humans' of the Heidelberg Academy of Sciences, Senckenberg Research Institute, Senckenberganlage 25, 60325, Frankfurt am Main, Germany

[6] Institut des Sciences de la Terre Paris, UMR 7193 ISTeP, CNRS-INSU, Sorbonne Université, Paris, France

Correspondence to: Maé Catrain (mae.catrain@edu.mnhn.fr)

Abstract. The major climate change recorded during the Early-Middle Pleistocene Transition (1.4-0.4 Ma) is characterized by an increase in the length of climatic cycles from 41 ka to 100 ka. During this period, the Mediterranean climate underwent aridification associated with a drop in temperatures. This period also corresponds to the arrival of the first hominins in Western Europe. This study aims to establish the climatic framework at the end of the Early Pleistocene between MIS 37-31 (~1.25 to 1.06 Ma). To this end, a multiproxy approach was applied to assemblages of planktonic foraminifera, pollen and clay mineralogy, constituting a multi-method approach to climate reconstruction. Comparisons with other sequences from the Central and Western Mediterranean show major differences between the Iberian Peninsula and southern Italy. Clay mineralogy analysis highlights a sudden change in oceanic and atmospheric circulation in the Alboran Basin around 1140 ka. Climate reconstructions follow climatic cycles, with temperatures that appear to be underestimated compared to temperature reconstructions based on fauna from southern Spain. Precipitation reconstructions, on the other hand, are more consistent, suggesting that the climate and vegetation of this region are more likely to be influenced by variations in precipitation. These new data enhance our understanding of the climate of the South-western Mediterranean at the beginning of the Early-Middle Pleistocene Transition.

1. Introduction

The boundaries of the Early Middle Pleistocene Transition (EMPT), also known as the Mid-Pleistocene Transition, have been set at 1.25 to 0.75 Ma by Clark et al. (2006). This chronological window has been widely discussed and

https://doi.org/10.5194/egusphere-2026-1342
Preprint. Discussion started: 18 March 2026

extended to 1.4 to 0.4 Ma by Head and Gibbard (2015). At that time, the Earth's climatic cycles lengthened from 41 kyr to 100 kyr (Pisias and Moore, 1981; Lisiecki and Raymo, 2005), and cycles became asymmetrical, with gradual onsets of glaciation and abrupt glacial terminations (Lisiecki and Raymo, 2005). This difference in structure is linked to a combination of changes in the influence of orbital parameters on the Earth's climate system, as well as internal changes involving feedback loops (Chalk et al., 2017; Head and Gibbard, 2015; Berends et al., 2021; Herbert, 2023). Before the EMPT, climate cycles were controlled by obliquity, whereas after the EMPT, they are often presented as being controlled by eccentricity. However, this cyclicity is much more complex, involving the influence of obliquity (41 ka), precession (23 ka) and an eccentricity cycle (100 ka) (Maslin and Brierley, 2015; Herbert, 2023). During the EMPT, the cooling trend that began in the Late Pliocene continued and accelerated in parallel with a decrease in the concentration of atmospheric CO_2 (Martínez-Botí et al., 2015). Glacial periods became more intense and longer (Herbert, 2023). The increase in cycle duration associated with the 100-ka cyclicity is recorded towards the end of the Early Pleistocene, between Marine Isotope Stages (MIS) 37 to 31 (1.24 to 1.06 Ma), comprising the particularly long MIS 36-35 cycle (~75 ka; Barker et al., 2022; Hodell et al., 2023). It is also marked by the MIS 31 'super interglacial' (DeConto et al., 2012; Melles et al., 2012) and the glacial MIS 34, which has recently been characterized as extreme cooling (Margari et al., 2023).

The EMPT coincides with the arrival of the first hominins in Western Europe, as shown by evidence of occupation dating to around 1.4-1.2 Ma in Italy and on the Iberian Peninsula (Peretto, 2006; Carbonell et al., 2008; Moyano et al., 2011; Duval et al., 2024; Cucart-Mora et al., 2026). The Mediterranean is a key area for discussing hominin diffusion, with regards to the archaeological evidence. In addition, the region is highly sensitive to climate change and is thus appropriate for cross-checking climate results from the high- and mid-latitude systems of the Northern Hemisphere and the African monsoon regimes. The impact of global climate change during the EMPT on the Mediterranean is still poorly understood due to the scarcity of reliable sedimentary archives for this region. Some previous studies have shown that aridification was a major parameter throughout this period, leading to changes in vegetation, including forest regression and expansion and the progressive disappearance of relict taxa with affinities for warm and humid environments (Joannin et al., 2011; Pross et al., 2015; Magri et al., 2017; Donders et al., 2021). Foraminifera assemblages reveal that changes in Mediterranean circulation, and particularly variations in Mediterranean outflow water (MOW), resulted in a modulation of Atlantic oceanic circulation, heat transport (Bahr et al., 2018, 2022) and ventilation (Guo et al., 2020). To date, changes in the atmospheric system based on the mineralogy of clays in the Mediterranean at the end of the Early Pleistocene are only continuously documented at ODP Site 964 (Ionian Sea) and MD 964 (Levantine Basin), in the Central and Eastern Mediterranean, respectively. Both records highlight changes in sedimentary sources, varying between North Africa and the southern Apennine Peninsula (Zhao et al., 2016), and changes in precipitation in the Nile source areas linked to monsoon activity (Zhao et al., 2012). Climate reconstruction efforts for this period are still in their infancy. Based on pollen assemblages, only three sequences have been used so far as supports for climate reconstruction at the end of the Early Pleistocene: Lake Acigöl in Türkiye (Robles et al, under revision), which covers the entire EMPT period, previous data from ODP 976 (Joannin et al., 2011) and the Palominas site (Altolaguirre et al., 2020), which covers the beginning of the transition. Other climate reconstructions based on faunal assemblages from Spanish archaeological and palaeontological sites also provide information on time windows, depending on site chronology: Gran Dolina (Blain et al., 2009), Fuente Nueva 3, Barranco Leon (Agustí et al., 2009; Blain et al., 2011, 2016; Saarinen et al., 2021; Sánchez-Bandera et al., 2023), and Almena-Casablanca

https://doi.org/10.5194/egusphere-2026-1342
Preprint. Discussion started: 18 March 2026

3 (Blain et al., 2007; Marquina-Blasco et al., 2025). Comparing different types of climate reconstruction (based on pollen and fauna) can yield a more complete picture of the climate. It is therefore essential to provide new long-term climate data in order to understand global and regional differences in the Mediterranean climate during the EMPT.

Despite the widespread use of marine sequences, the possibilities for studying climate change throughout this period with a multiproxy and integrated approach are limited by the restricted number of long sequences covering the entirety of the EMPT. Thus, our knowledge of the EMPT climate is fragmentary, and questions persist as to the impact of the EMPT on hydroclimatic dynamics, terrigenous sources and vegetation changes. How did the different basins of the Mediterranean respond to climatic changes during the EMPT? And how did this transition begin in the Mediterranean?

This study proposes the first multiproxy and multi-method analysis covering the period ranging from MIS 37 to 31 (1.24 to 1.06 Ma) in the Western Mediterranean using the ODP 976 marine sequence (Alboran Sea). It connects isotope records, pollen data (Joannin et al., 2011; Catrain et al., 2025), planktonic foraminifera assemblages, clay mineralogy and climate reconstructions based on foraminifera to obtain Sea Surface Temperatures (SSTs) and based on pollen data to reconstruct mean air temperatures and precipitation. For this time period, comparisons with the sites of Montalbano Jonico in south Italy (Joannin et al., 2008; Girone et al., 2013), Monte San Giorgio in Sicily (Catrain et al., 2025) and Palominas in southern Spain (Altolaguirre et al., 2020) will produce the first sea-continent environmental and climatic outline. This approach aims to enhance our understanding of climate system variability through: i) examining links between sea and continent, ii) a regional focus and comparison of climate response in the Central and Western Mediterranean, and iii) a methodological discussion of pollen-based climate reconstruction methods.

2. Environmental setting

According to the Köppen classification, the Mediterranean climate is a temperate climate characterized by dry summers (Cs) with precipitation mainly concentrated in winter. Some areas are characterized by more arid steppe (BS) and desert (BW) climates (Köppen, 1936; Daget, 1977; Quézel and Médail, 2003; Peel et al., 2007; Beck et al., 2023). Current annual rainfall around the Alboran Sea varies between 200 mm and 1100 mm and annual temperatures between 12 and 19°C, depending on areas and altitudes (Fig.1). The surface circulation of the Alboran Sea is linked to the entry of the Atlantic jet (AJ) and two main surface gyres: the Western Alboran Gyre (WAG) and the Eastern Alboran Gyre (EAG), both with an anticyclonic circulation. The WAG and EAG are connected to each other by a smaller gyre; the Central Cyclonic Gyre (CCG) (Fig.1.A) (Sánchez-Garrido and Nadal, 2022). The surface waters from the Atlantic Ocean entering through the Strait of Gibraltar move towards the Almeida Oran Front (AOF) where they mix with saltier waters. From the east, the Levantine Intermediate Water (LIW) and the colder and more saline Western Mediterranean Deep Water (WMDW) move west before leaving through the strait. The mixing of these two water masses upon arrival in the Atlantic Ocean is called Mediterranean Outflowing Water (MOW) (Fig.1.B) (Fabres et al., 2002; Macías et al., 2008; Moreno et al., 2005; Pérez-Folgado et al., 2003; Tintore et al., 1988).

https://doi.org/10.5194/egusphere-2026-1342
Preprint. Discussion started: 18 March 2026

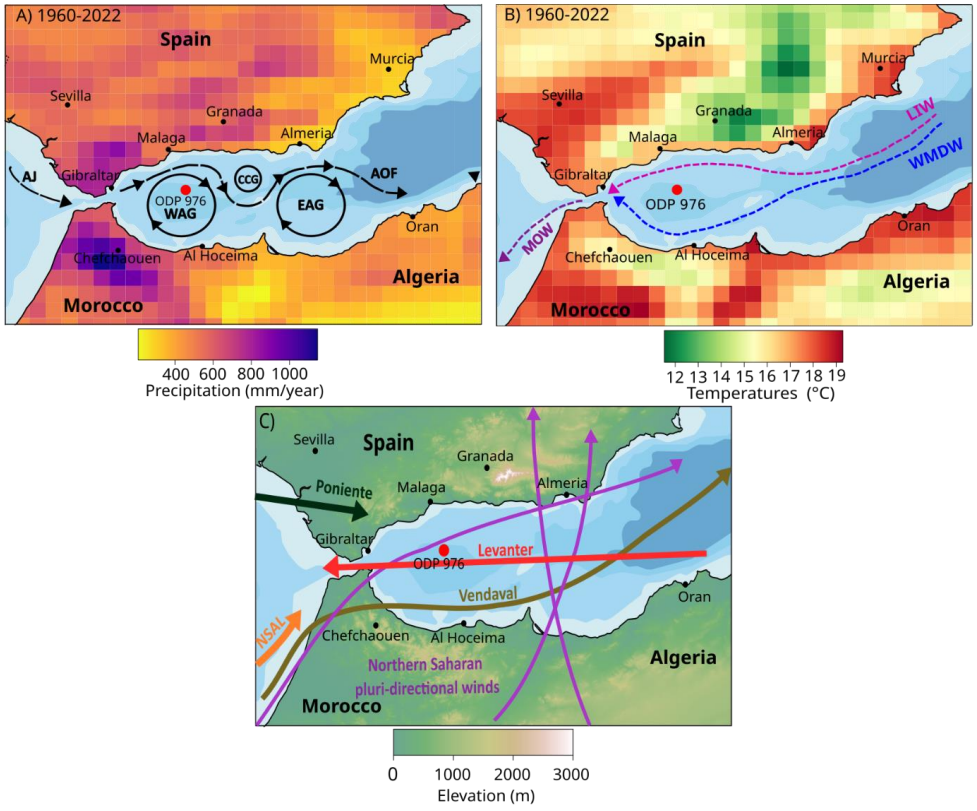

Figure 1. ODP site 976 climate and location maps. Climate data from ERA5 reanalysis between 1960-2022 with a lat-lon grid of 0.25 degrees. A) Mean annual precipitation with sea surface circulation. AJ: Atlantic Jet, WAG: Western Alboran Gyre, CCG: Central Cyclonic Gyre and EAG: Eastern Alboran Gyre. B) Mean annual temperature with sea deep circulation. MOW: Mediterranean Outflow Water, LIW: Levantine Intermediate Water and WMDW: Western Mediterranean Deep Water. C) Atmospheric circulation. NSAL: Northern Saharan Air Layer.

In the Western Mediterranean region, atmospheric circulation is influenced by the westerlies and variations in the positioning of the intertropical convergence zone and therefore the monsoon system. The Western Mediterranean is subject to winds from Africa, such as Northern Saharan pluri-directional winds, which originate in the Sahara. On the Atlantic side, the Saharan Air Layer (SAL) originating from the monsoon system is deflected by the Azores high pressure system, thus creating the northern branch of the SAL (NSAL), which goes up to the Western Mediterranean (Bout-Roumazeilles et al., 2007; Leblanc, 2022). The Alboran basin is subject to westerly and south-westerly winds, the Poniente and the Vendaval, and warm easterly winds such as the Levanter.

Around the Alboran Sea, Mediterranean vegetation is organized altitudinally according to temperature and precipitation distribution. The Thermo-Mediterranean belt (0 to 300-700 m) is mainly composed of Mediterranean species, such as olive trees (*Olea*), pistachio trees (*Pistacia*) and carob trees (*Ceratonia*). The Meso-Mediterranean (300-700 to 1000-1200 m) and Supra-Mediterranean (1000-1200 and 1500-1700 m) belts consist of evergreen mixed forest and deciduous oak (*Quercus*) and pine (*Pinus*) forests respectively. Above these

https://doi.org/10.5194/egusphere-2026-1342
Preprint. Discussion started: 18 March 2026

altitudes, forests are composed of conifers such as pine (*Pinus*), fir (*Abies*) and cedar (*Cedrus*) in Morocco (Benabid, 1985; Ozenda, 1994; Quézel and Médail, 2003; Médail, 2022).

3. Materials and Methods

3.1. Site location and chronology

ODP Leg 161 site 976 (36°12.30'N, 4°18.8'W, 1108 m b.s.l. (below sea level); Fig. 1) is located in the northwest of the Alboran Sea. The sediment core records a continuous lithostratigraphy from the Upper Miocene to the Holocene (Comas et al., 1996). Our study focuses on the depth interval of the master core from 281.23 to 256.53 mcd (metre composite depth), corresponding to the MIS 37-31 interval, with an age model based on nannofossil events, sapropel and the correlation between ODP site 976 (Catrain et al., 2025) and global stack oxygen isotope curves (Lisiecki and Raymo, 2005). The sedimentary sequence consists of homogeneous clays rich in nannofossils and silty nannofossils. The lithogenic particles in the Alboran Sea come from aeolian and fluvial sources from Spain and Morocco.

3.2. Palynological analysis

The palynological analysis was based on a standard protocol with HF (70%) and HCl (37%) attacks. A minimum of 150 grains excluding *Pinus* (overrepresented) and a minimum of 15 taxa were recorded. A total of one hundred and twenty-two samples were counted along the MIS 37-31 interval. Two sums are defined to calculate the percentages: the Main Pollen Sum (MPS), which excludes Pteridophyte spores, *Pinus* and aquatic plants, and the total sum of palynomorph grains (TSP), which includes all the pollen grains and pteridophyte spores. Percentages are calculated using the MPS, except for *Pinus*, aquatic plants and fern spores, for which the TSP is used. Data are presented in the form of a pollen diagram plotted with the Tilia software (version 3.0.1; Grimm (1991)). For comparisons between sites ODP 976 and Montalbano Jonico, the sum is calculated in the same way and the ecological groups correspond to those defined by Catrain et al. (2025).

3.3. Planktonic foraminifera analysis and isotope analysis

Planktonic foraminifera analysis was carried out on one hundred and sixteen samples with a spacing of 10 cm to 80 cm, with an average of every 23 cm. The sediments were sieved to 150 µm. Foraminifera were counted using a binocular magnifying glass with a minimum of 450-500 tests per sample to be representative. Identification is based on publications (Orbigny, 1839) and a book (Schiebel and Hemleben, 2017).

Between eight and 12 individuals of the foraminifera *Globigerina bulloides* were selected from 56 of these same samples to conduct $\delta^{18}O$ and $\delta^{13}C$ analyses. The samples were cleaned with methanol before being inserted into the dual-entry Isoprime isotope ratio mass spectrometer. Analyses were performed at the Laboratory for Sciences of Climate and Environment (LSCE, France) on the analytical platform PANOPLY.

3.4. Clay mineral analysis

Clay mineral associations were studied using X-ray diffraction following the protocol of Bout-Roumazeilles et al. (1999). In this study, ‘clay minerals’ refer to the main phyllosilicate minerals in the clay-size fraction (generally less than 2-µm particles). All samples were first decalcified with 0.2 M HCl, before clay defloculation by successive washing with distilled water. The clay-size fraction was separated by settling according to Stokes's

https://doi.org/10.5194/egusphere-2026-1342
Preprint. Discussion started: 18 March 2026

law, concentrated by centrifugation, and oriented by wet smearing on glass slides. X-ray diagrams were obtained using a Bruker D4 Endeavor diffractometer with CuKα radiation and a Ni filter, coupled with a Lynxeye detector. A tube voltage of 30 kV and a tube current of 35 mA were utilised. Three X-ray diagrams were performed: air-dried sample (normal run), ethylene-glycol vapour saturation for 12 h (glycol run) and heating at 490°C during 2 h (heating run). The goniometer scanned from 2.49° to 32.49° 2θ for normal and glycol run and from 2.5 to 14.5° 2θ heating run. Each clay mineral is characterized by its basal layer plus interlayer interval (d), as revealed by XRD analysis (Brown and Brindley, 1980). Smectite (S) is characterized by a peak at 14 Å on the normal run, which expands to 17 Å after saturation by ethylene-glycol and retracts to 10 Å after heating. Illite (I) presents a basal peak at 10 Å on the three runs. Palygorskite (P) is characterized by the presence of a peak at 10.34Å on the normal run. Chlorite (C) is characterized by peaks at 14 Å (001), 7 Å (002), 4.75 Å (003) and 3.53 Å (004) on the three runs. Kaolinite (K) is characterized by peaks at 7 Å (001) and 3.58 Å (002) on the normal and glycol runs. Both peaks disappear or are strongly reduced after heating. To distinguish kaolinite from chlorite, the portion of the spectrum containing the basal peaks of kaolinite (002) and chlorite (004) around 3.55 Å is step-scanned in a high-resolution mode following standard procedures described in detail by Petschick et al. (1996). Semi-quantitative estimation of clay mineral abundance is based on peak areas and totalled to 100% (S + I + K + C + P = 100%). Peak area measurements were taken in the glycol runs using the Macintosh MacDiff® 4.2.5 software (Petschick, 2000). The error on measurement reproducibility is estimated to be ±5% for each clay mineral.

3.5. Sea surface temperature reconstruction from planktonic foraminifera

Sea surface temperatures (SST) were reconstructed based on planktonic foraminifera assemblages, using PaleoAnalogs software (version 3.0). This software uses the Modern Analogue Technique (MAT), which compares a database of modern assemblages with fossil assemblages to find the closest modern samples (Theron et al., 2003). The degree of dissimilarity between samples is calculated using the Squared-Chord-Distance. A minimum of ten temperature analogues were selected and then averaged to estimate those of the fossil samples. Reconstructions were based on a North Atlantic Mediterranean database (Siccha and Kucera, 2017).

3.6. Pollen-inferred climate reconstructions

For climate reconstructions, pollen counts were used to reconstruct four climatic parameters: Mean Annual Air Temperature (MAAT), Mean Temperature of the Coldest month (MTCO), Mean Temperature of the Warmest month (MTWA), and Mean Annual Precipitation (PANN). A multi-method approach was adopted for greater reliability (Peyron et al., 2011, 2013; Salonen et al., 2019; Chevalier et al., 2020), and taxa that have now disappeared from the Mediterranean (relict taxa) were included in certain methods (Fauquette et al., 1998). Five methods with different mathematical bases were selected: the modern analogue technique (MAT; (Guiot, 1990)), weighted averaging partial least-squares regression (WAPLS; (Ter Braak et al., 1993)), random forest (RF; (Breiman, 2001; Prasad et al., 2006)), boosted regression trees (BRT; (De'ath, 2007; Elith et al., 2008)) and the climatic amplitude method (CAM; (Fauquette et al., 1998)).

MAT works in a similar way to foraminifera. WAPLS is a non-linear regression technique that creates relationships between climate parameters and pollen taxa within the modern database, then applies them to fossil

https://doi.org/10.5194/egusphere-2026-1342
Preprint. Discussion started: 18 March 2026

assemblages (Ter Braak et al., 1993; Chevalier et al., 2020). RF and BRT methods are based on machine learning and have recently been used for palaeoclimatology in Northern Europe (Salonen et al., 2019) and the Mediterranean Basin (d'Oliveira et al., 2023, 2025; Robles et al., 2023, 2025; Sassoon et al., 2025; Charton et al., 2025). For RF, each tree is estimated from a random set of different subsets defined separately from the modern data assembly. This is called bootstrapping and each sample has the same probability of being selected (Breiman, 2001; Prasad et al., 2006). For BRT, the random creation of sets from modern assemblages means that samples that were not sufficiently taken into account in the previous tree have a higher probability of being selected in the next training sessions. This is known as boosting (De'ath, 2007; Elith et al., 2008). The MAT and WAPLS methods were applied with the R *rioja* package (Juggins, 2024), RF with *randomForest* package (Breiman et al., 2024) and BRT with *dismo package* (Hijmans et al., 2024).

The Eurasian and Mediterranean Current Surface Sample Database (EAPDB; n = 3373 sites), compiled by Peyron et al. (1998, 2011, 2013), and completed by Dugerdil et al. (2021) and Robles et al. (2023), was used for the first four methods. In this dataset, each sample is associated with a biome (Tarasov et al., 1998; Elenga et al., 2000). Some biomes were selected and others were not taken into account in order to better constrain the database: cold deciduous forest (CLDE), cold desert (CODE), cool mixed forest (COMX), cold steppe (COST), hot desert (HODE), pioneer (PION), temperate deciduous forest (TEDE), warm mixed forest (WAMX), warm steppe (WAST) and xerophilous (XERO). One hundred and seven sites from the Eurasian modern database (EMPD) (Davis et al., 2020) were added to the EAPDB for a more reliable representation of certain taxa (Ericaceae). Particular attention was paid to these new samples to avoid selecting anthropized sites. *Pinus*, kept in the modern database, was not included in the fossil sequence due to its overrepresentation, except for the Palominas site which corresponds to a continental basin.

The CAM is based on the overlap of the climatic requirements of taxa and takes relict taxa into account. The climatic requirements of ~135 taxa were defined on the basis of 8000 modern spectra and the literature. The past climate is estimated by transposing the climatic requirements of the maximum number of modern taxa to the fossil data, and the most probable climate corresponds to the suitable climatic interval for the highest number of taxa and to a 'Most Likely Value' corresponding to a weighted mean (Fauquette et al., 1998). Some taxa represented by a single grain in the record (*Lygeum, Croton, Rhus, Myrthus, Calligonum, Taxodium*, and Sapotaceae) and Cichorioideae were not taken into account in the climate reconstruction as they generate noise.

These climate reconstruction methods were applied to our ODP site 976 sequence, as well as to the sites of Palominas and Monte San Giorgio, for comparison. For the CAM, Poaceae were not taken into account for the reconstruction of the Palominas site for the same reason as for Cichorioideae in ODP site 976.

3.7. PERMANOVA

PERMANOVA is a non-parametric test based on the F-test. The p-value of PERMANOVA is estimated by permutation, which makes it particularly well adapted to data that do not follow multivariate normality or homogeneity of variances, as is the case with climate reconstruction data. These two criteria are important for the application of traditional analyses of variance methods (ANOVA, MANOVA), as confirmed using a Mardia test. Whilst ANOVA compares group means to verify whether or not they come from the same population, PERMANOVA projects data points into measured space, and therefore compares group centroids instead of means. When the p-value of PERMANOVA is less than or equal to 0.05, the test is significant and rejects the null

https://doi.org/10.5194/egusphere-2026-1342
Preprint. Discussion started: 18 March 2026

hypothesis, which verifies whether group averages come from the same population or reflect changes. This test was applied to reconstructed temperature and precipitation data, which were centred and reduced to avoid the influence of scale and give equal weight to each variable and to compare trends.

4. Results

4.1. Late Early Pleistocene vegetation record around the Alboran Sea

The pollen data presented by Catrain et al. (2025) are composed of 31 families and 72 genera distributed over the different belts of Mediterranean vegetation. The temperate taxa curves, mainly represented by the *Quercus* deciduous type, *Isoetes* and elements of steppe environments (*Artemisia*, Amaranthaceae, *Ephedra*) highlight alternating warm/ humid periods and cold/dry periods between MIS 37 and 31. The high percentages of high-altitude forest elements, such as *Cedrus* and *Abies*, and of Ericaceae, point to the onset of colder but still humid climatic conditions at the end of the interglacial. The constant values of Asteroideae, Cichorioideae and Poaceae show a continuous presence of an open vegetation environment (Fig.2).

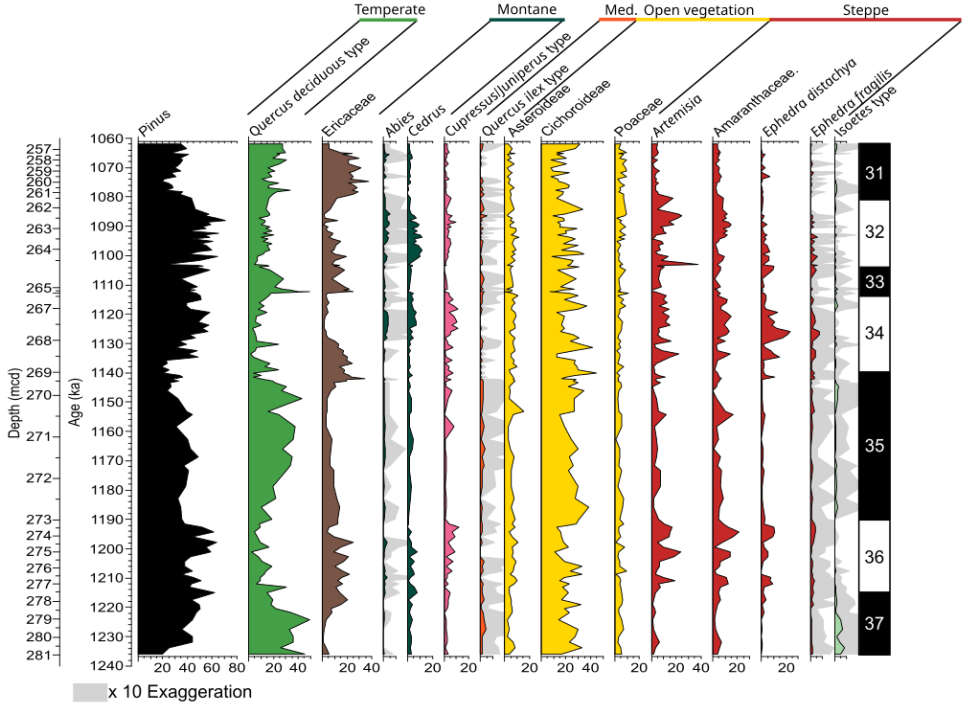

Figure 2. Simplified palynological diagram from ODP site 976 associated with the MIS chronology. The ecological groups are those defined by Catrain et al. (2025)

4.2. Late Early Pleistocene planktonic foraminifera assemblages and SST reconstruction

Altogether, ninety-seven samples were analysed. However, fourteen samples could not be used due to the low number of foraminifera. Thirty-nine species were identified, dominated by *Neogloboquadrina incompta* (on

https://doi.org/10.5194/egusphere-2026-1342
Preprint. Discussion started: 18 March 2026

average 30%), *Globigerina bulloides*, *Globorotalia inflata*, *Neogloboquadrina pachyderma*, and *Globigerinoides ruber* white (Fig. 3). *Globigernella calida* (around 1%), *Globigerinita glutinata* (4%), and *Globigerina falconensis* (3%) are consistently present. Taxa with affinity for warm waters, such as *Orbulina*, *Globorotalia crassaformis*, and *G.calida*, are poorly represented in the assemblage. Warm taxa, *Globigerinoides ruber* white type, and taxa with an affinity for temperate waters, such as *Globigerina bulloides* and *Globorotalia inflata*, are found in interglacial periods. Two peaks of *G Globigerinoides ruber* white are recorded at 1229 ka (39%) and 1084 ka (49%). *Turborotalita quinqueloba* develop significantly (up to 30%) between 1215 and 1200 ka. The high *Neogloboquadrina pachyderma* values, with peaks between 40 and 70%, are synchronized with glacial periods.

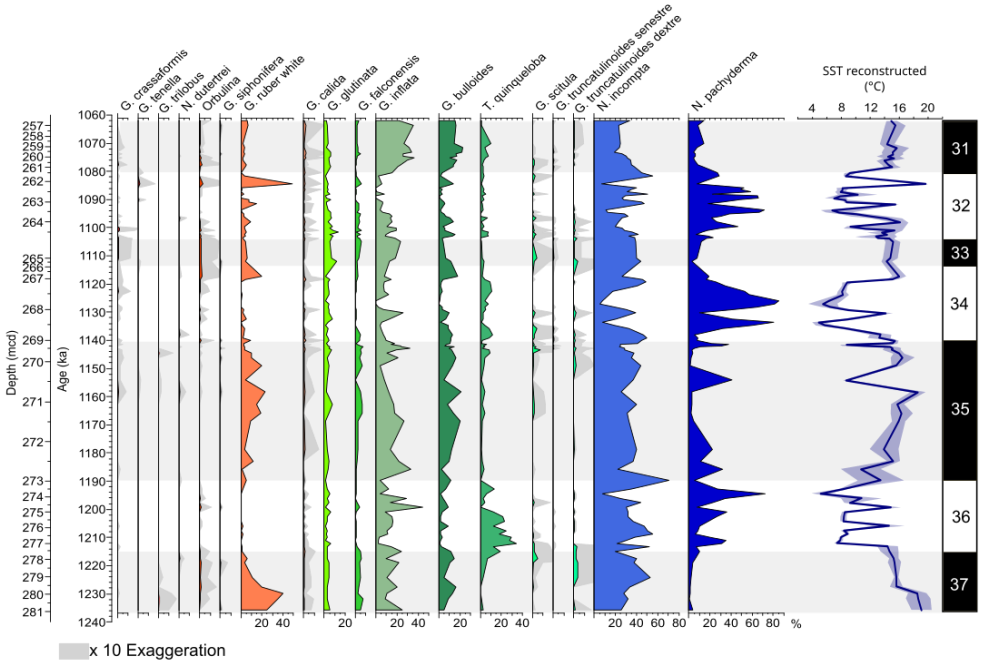

Figure 3. Planktonic foraminifera assemblages from ODP site 976 and SST reconstructed with the Modern Analog Technique (MAT) associated with MIS chronology. The red curves correspond to foraminifera with warm affinities and the blue curves to cold affinities.

Mean annual sea surface temperature values reconstructed from planktonic foraminifera assemblages vary between 5 and 19.6 °C. The values show marked variation with a trend of cooling during glacial periods and warming during interglacial periods (Fig. 3).

4.3. Late Early Pleistocene clay analysis in the Alboran Sea

The clay mineral signals can be divided into five main phases of variation between stages 37 to 31 (Fig. 4):

- Phase I records very little fluctuation in each clay mineral: palygorskite (~7%), kaolinite (~17%), chlorite (~17%), illite (~40%) and smectite (~20%). The I/K ratio is around 2.4.

https://doi.org/10.5194/egusphere-2026-1342
Preprint. Discussion started: 18 March 2026

- Phase II is the shortest phase at the end of stage 37 and corresponds to an increase in kaolinite (~20-21%), a lesser increase in chlorite (~19%) and a decrease in smectite (~12%) and the I/K ratio (~2).

- Phase III is the longest phase, covering MIS 36-35, and records fairly constant values for each mineral, very similar to those for phase I.

- Phase IV, which begins with the transition from MIS 35 to 34, shows the greatest change in clay composition. A general decreasing trend is observed for illite (~31%), kaolinite (~10%), chlorite (~11%) and palygorskite (~6%), although the latter peaks at around 1114, 1103, 1001 and 1088 ka. On the other hand, during this phase, smectite increases significantly, reaching average values of around 42%. The I/K ratio fluctuates more regularly, with values rising slightly to 3.69.

- Phase V presents a return to the values of phases III and I.

- Phase VI shows a new smectite peak with similar values to those for phase IV.

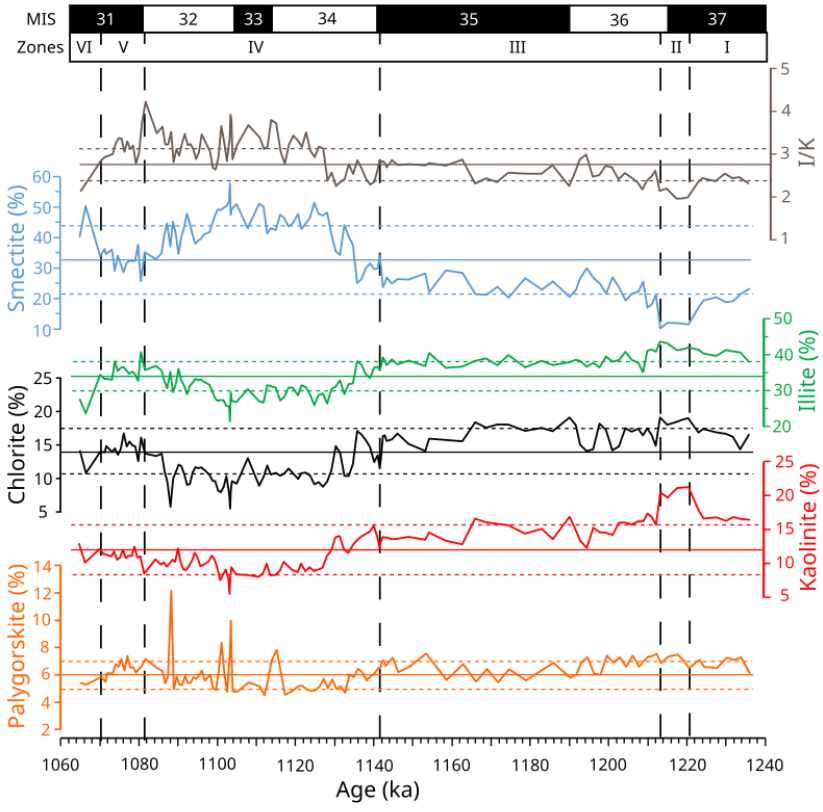

Figure 4. Clay mineralogy from ODP site 976 associated with MIS chronology. Solid lines represent the mean and dotted lines the standard deviation.

https://doi.org/10.5194/egusphere-2026-1342
Preprint. Discussion started: 18 March 2026

4.4. Climate reconstruction during the Late Early Pleistocene

Reconstructions from pollen data at ODP site 976 show similar trends between all the different methods and for each parameter (Fig 5). BRT and MAT have the best R^2 and RMSE, while WAPLS yield the poorest for all climatic parameters (Table 1). MAT and WAPLS show greater variation amplitude than BRT, RF and CAM, where differences between warm, wet phases and cold, dry phases are less pronounced. Parameter variations follow those of interglacial and glacial periods. Interglacial phases are characterized by higher temperatures and precipitation than for glacial periods. RF appears colder than other methods, with a general trend of around 10 °C in MAAT and 0 °C for MTCO. WAPLS and MAT present more humid conditions.

MIS 37 (1245-1215 ka) shows MAAT values of around 13 °C for MAT and WAPLS, ~12 °C for CAM and BRT, and finally 10 °C for RF. For MTWA, temperatures oscillate around two values: ~22 °C for MAT, CAM and WAPLS, and 20-19 °C for the other two methods. For MTCO, RF has a lower average of around 0.6 °C, while BRT and WAPLS reconstruct temperatures of around 5 °C, as opposed to 4 °C with MAT and 3.4 °C with CAM. WAPLS and MAT record the highest rainfall with 788 and 727 mm/year, while BRT shows the lowest, at around 506 mm/year.

For glacial MIS 36 (1215-1190 ka), the reconstructed MAATs are around 12.5 °C (BRT), 11.5 °C (CAM and WAPLS), 10.3 °C (MAT) and 9 °C (RF). Temperatures for the warmest month are around 21 °C for CAM, MAT and WAPLS, and around 20 °C for RF and BRT. For the coldest month, BRT reconstructs the warmest temperatures around 4.3 °C, and RF and MAT the coldest, with values between 1 and -0.5 °C. CAM and WAPLS are around 2.5 °C. WAPLS is the highest for precipitation with 676 mm, followed by RF (628 mm) and CAM (572 mm), while MAT and BRT have the coldest values with 487 and 455 mm.

For MIS 35 (1190-1141 ka), annual temperatures around 13°C are associated with WAPLS, around 12.5 °C with MAT and BRT, around 11.5°C with CAM and around 10.3°C with RF. The MAT MTWA is around 23 °C, 22 °C for WAPLS, 21 °C for CAM and 20 °C for BRT and RF. RF always has the coldest MTCO values, by around 0.7 °C. WAPLS and BRT are the warmest, around 5 °C. CAM and MAT are around 3 °C. As with the two previous MISs, WAPLS is the wettest (754 mm) and BRT is the driest (464 mm). For RF, MAT and CAM, precipitation varies between 654 and 613 mm.

Between 1141 and 1114 ka (MIS 34), BRT yields the highest reconstructed MAAT , around 12 °C, and RF the lowest, around 9 °C . The other three methods are around 11 °C. MTWA are either around 21 °C (CAM, MAT and WAPLS) or 20 °C (BRT and RF). For MTCO, the lowest values are those of MAT and RF (-1 °C), and the highest are WAPLS and BRT (3 °C). PANNs for WAPLS are around 691 mm, around 622 mm for RF, around 591 mm for CAM, around 503 mm for MAT, and the lowest at around 433 mm for BRT.

During MIS 33 (1114-1104 ka), MAATs varied between 13°C (WAPLS) and 10 °C (RF). For BRT, MAAT was approximately 12 °C and 11 °C for the last two methods. For MTWAs, all methods were around 21°C except RF, which was around 19 °C. For the coldest month, BRT and WAPLS are the warmest with ~4.4°C and RF is the coldest at around 0 °C. For precipitation, WAPLS is always the wettest (800 mm) and BRT is the driest (493 mm). The other three methods are between 668 and 646 mm.

For MIS 32, BRT was the warmest (1104–1081 ka), at around 12 °C, and RF the coldest at around 9 °C in terms of MAAT. The MTWA of WAPLS, MAT and CAM are around 21 °C, and for BRT and ka RF they are around 20 °C. For MTCO, the lowest value is -2 °C (MAT) and the highest is 3 °C (BRT). WAPLS is around 2

https://doi.org/10.5194/egusphere-2026-1342
Preprint. Discussion started: 18 March 2026

°C, CAM is close to around 2.5 °C and RF is lower at around -1 °C. Precipitation for WAPLS is around 898 mm, approximately 451 mm for BRT, and close to 600 mm again for the other three methods.

The last interglacial MIS 31 (1081-1062 ka) is marked by annual temperatures around 12 °C (BRT and WAPLS), 11 °C (CAM and MAT) and 10 °C (RF). Reconstructed MTWAs are mainly around 20 °C for RF, BRT and WAPLS. CAM is the warmest at around 22°C, followed by MAT at around 21°C. MTCO amplitude varies between 5 °C for WAPLS and 0 °C for RF. For PANN, WAPLS is always the wettest at around 851 mm and BRT is always the driest at 492 mm. RF and CAM are close at around 660 mm and MAT is slightly wetter at around 787 mm.

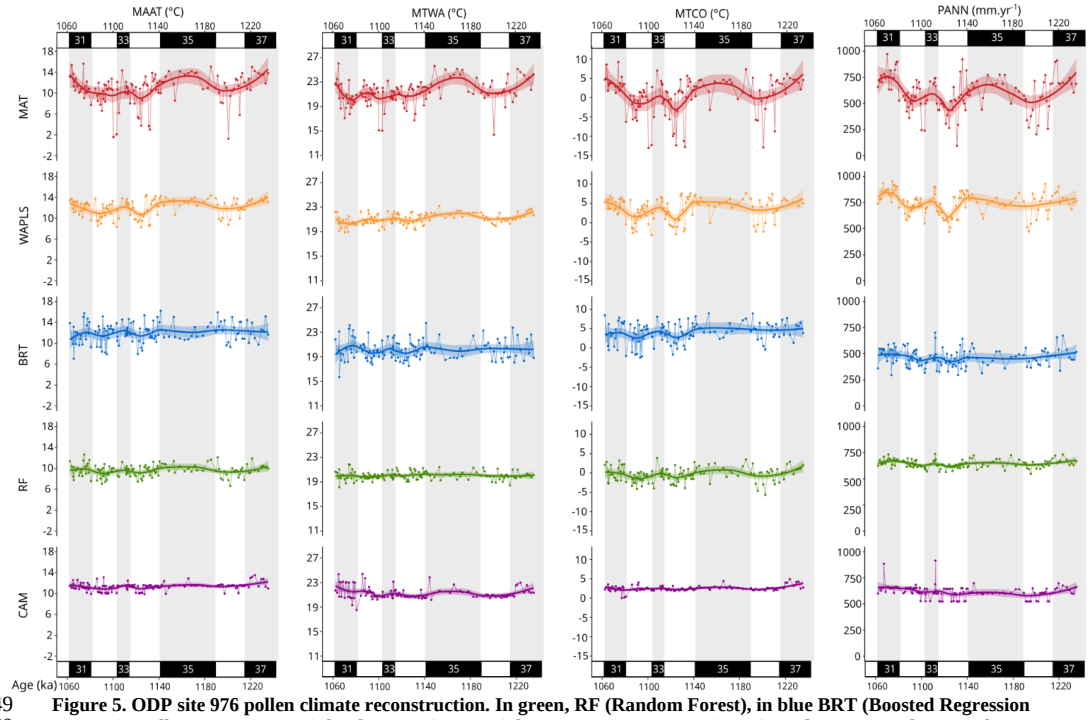

Figure 5. ODP site 976 pollen climate reconstruction. In green, RF (Random Forest), in blue BRT (Boosted Regression Trees), in yellow WAPLS (Weighted Averaging Partial Least Squares regression), in red MAT (Modern Analogue Technique) and in purple CAM (Climatic Amplitude Method). Four climatic parameters: MAAT (Mean Annual air Temperature), MTWA (Mean Temperature of the WArmest month), MTCO (Mean Temperature of the COldest month) and PANN (mean annual precipitation). Grey bands correspond to interglacial periods and the thick coloured lines correspond to loess-smoothed curves and shaded areas to the 95 % confidence interval.

Table 1. R^2 (Pearson correlation coefficient) and RMSE (Root Mean Square Error) values for climatic parameters. The lower the RMSE and the higher the R2, the closer the method is to the target value from the modern database.

R^2	MAT	WAPLS	RF	BRT	CAM
MAAT	0.83	0.65	0.71	0.81	0.87
MTWA	0.79	0.54	0.62	0.70	0.68

https://doi.org/10.5194/egusphere-2026-1342
Preprint. Discussion started: 18 March 2026

MTCO	0.87	0.70	0.77	0.87	0.86
PANN	0.72	0.46	0.60	0.71	0.45
RMSE					
MAAT	2.53	3.30	2.92	2.36	3.4
MTWA	2.38	3.17	2.81	2.24	2.9
MTCO	3.30	4.53	3.88	2.95	5.5
PANN	194.25	241.41	204.44	176.96	257

4.5. Statistical analysis of climate reconstruction

The various tests carried out with PERMANOVA on the centred and reduced climate reconstruction data show that the methods are adequate. PANN is similar for all the methods from MIS 37 to MIS 33 (Fig 6). For MIS 32, only CAM has a p-value < 0.05 and is significantly different to MAT (p-value 0.004), WAPLS (p-value 0.004) and BRT (p-value 0.005). RF differs from MAT (p-value 0.039) and BRT (p-value 0.049) during MIS 31. For MAAT, all the methods for each period are similar (Fig 6).

PERMANOVA tests, however, show that all interglacial and glacial phases are different from the others, regardless of the methods, with p-values lower than 0.05 (Fig.7).

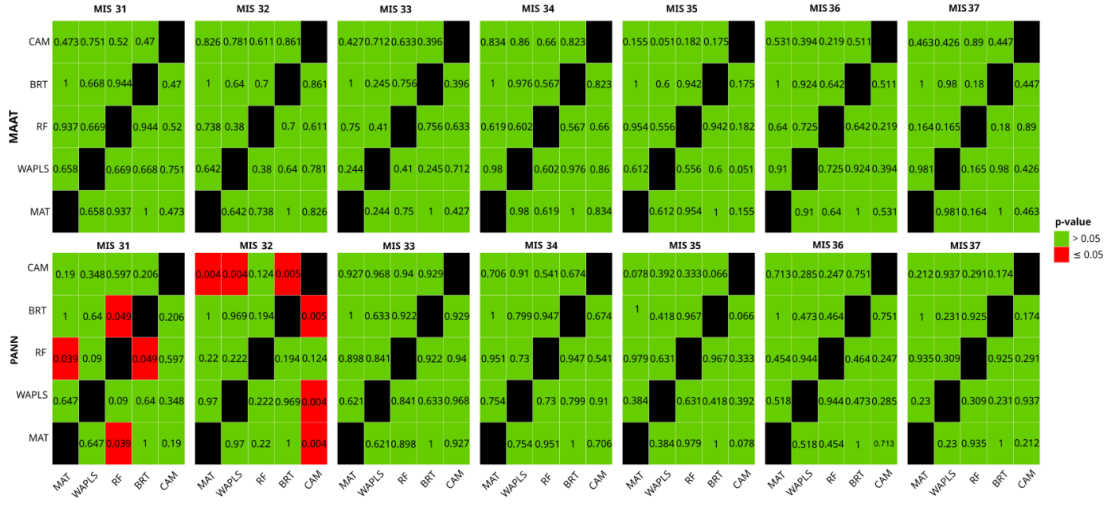

Figure 6. **PERMANOVA p-values between climate reconstruction methods for each isotopic stage and for Mean Annual Air Temperature (MAAT) and Mean of Annual Precipitation (PANN). A p-value less than or equal to 0.05 is significant and indicates that the two methods are different from each other.**

https://doi.org/10.5194/egusphere-2026-1342
Preprint. Discussion started: 18 March 2026

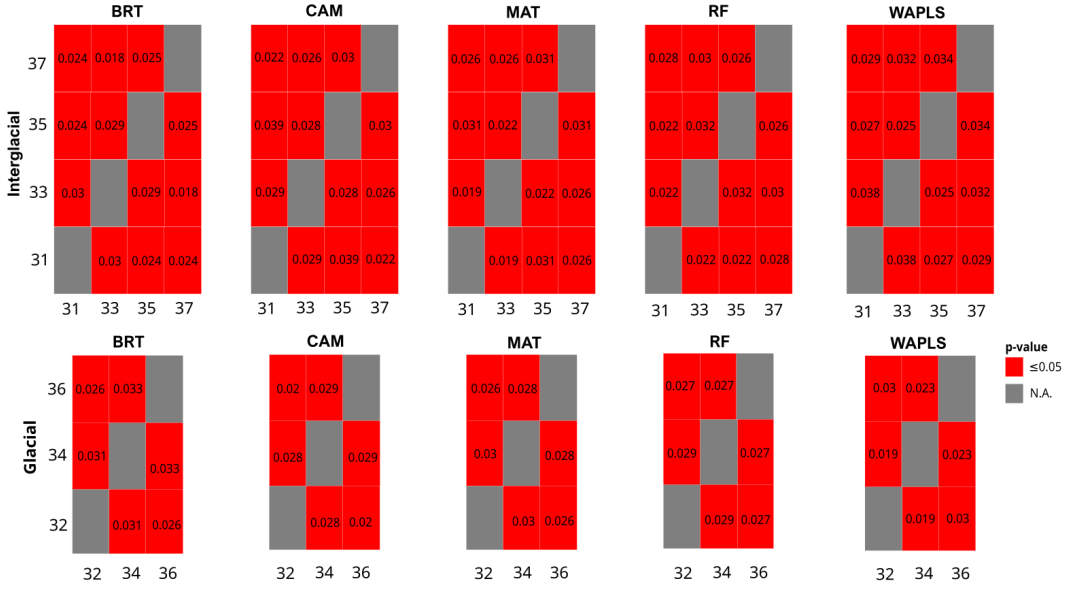

Figure 7. PERMANOVA p-values between the same types of periods (glacial-glacial and interglacial-interglacial) for each climate reconstruction method on centred-reduced data. A p-value less than or equal to 0.05 is significant and indicates that the two periods are different from each other.

5. Discussion

5.1. Land-sea responses from the Western to Central Mediterranean

Planktonic foraminifera data from the same marine sequence as the pollen data highlight simultaneous changes in oceanic characteristics and in the floristic composition of terrestrial ecosystems. The Mediterranean Basin, and in particular the Western Mediterranean, only comprises rare sites combining these two proxies. This foraminifera/pollen data approach is recorded in the Montalbano Jonico site over a large EMPT time window (Joannin et al., 2008; Girone et al., 2013).

Between MIS 37 and MIS 31 in ODP site 976 (Western Mediterranean basin), all the proxies highlight the typical interglacial and glacial variations recorded during this period, except clay mineralogy, which shows longer cycles. The comparison between pollen data and planktonic foraminifera assemblages highlights a synchronization of steppe elements with the polar affinity foraminifera *Neogloboquadrina pachyderma*. A similar pattern is observed during MIS 20-19 (Toti et al., 2020). This correlation emphasizes that the steppes from the Iberian Peninsula and/or North Africa are not only linked to aridity but also to low temperatures (Fig.8.a). The constant dominance of the subpolar affinity *Neogloboquadrina incompta* signal (~30%) throughout the period also attests to relatively cool surface waters (average SST of 12 °C). Air and ocean temperatures (MAAT and SST) reconstructed from pollen and planktonic foraminifera also show these glacial-interglacial variations (Fig. 8.a). The SST signal is highly influenced by the quantity of *Globigerinoides ruber* of subtropical affinity during interglacial phases, and *Neogloboquadrina pachyderma* of polar affinity, during glacial phases. For both air and ocean temperatures, these are lower than modern values. The current SST is 17.7 °C between 1981-2010 (36°N,03°W; (Guijarro et al., 2015; Sánchez-Laulhé et al., 2021)) and the current mean air annual temperature in

https://doi.org/10.5194/egusphere-2026-1342
Preprint. Discussion started: 18 March 2026

a perimeter of 400 km around ODP 976 is 16.8°C between 1960-2022 (calculated with ERA5 reanalysis). Furthermore, multiproxy analyses from ODP site 976 show that the warmest phase is MIS 37 (1245–1215 ka). During this phase, temperate forests reached their maximum development, averaging 35%, while steppes were reduced to 10%. This stage also has the highest percentages of *Globigerinoides ruber* (~20%), a warm-water foraminifera, and SSTs around 16.5 °C, as well as low $\delta^{18}O$ values (~0.56‰; Catrain et al., 2025) (Fig. 8).

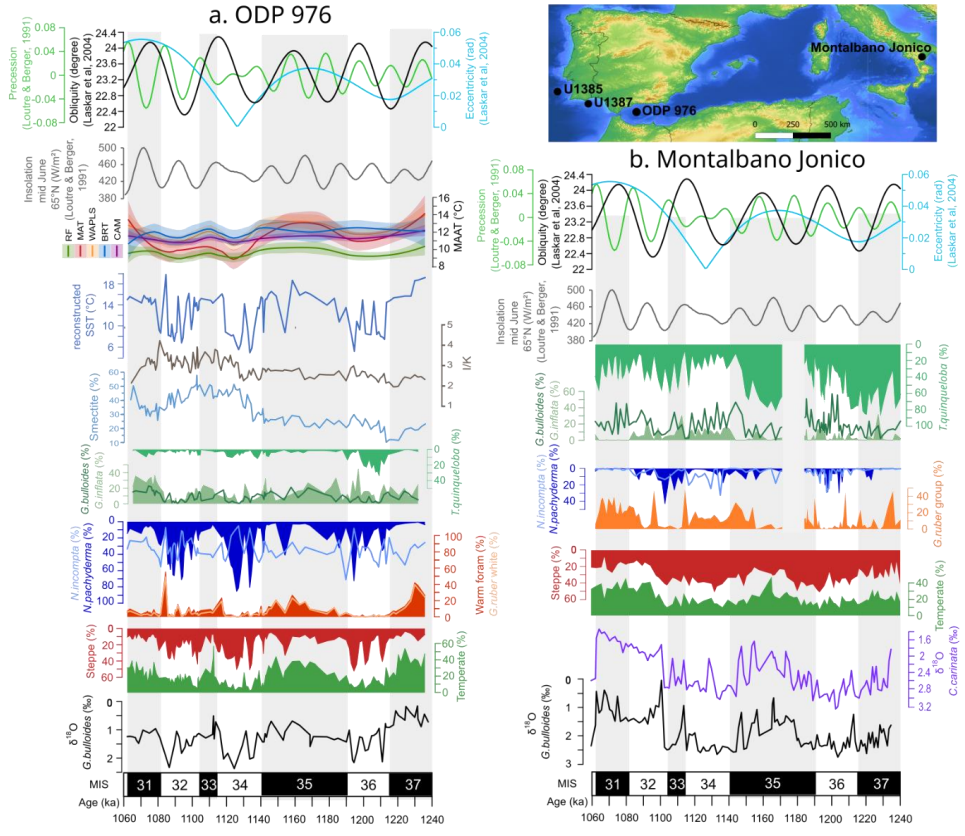

Figure 8. Land-sea variability comparison at ODP site 976 (left), compared to the site of Montalbano Jonico (right) in southern Italy. Isotope data for the ODP site 976 are from Catrain et al. (2025). For the Montalbano Jonico site, pollen and oxygen isotope data come from Joannin et al. (2008), and planktonic foraminifera data from Girone et al. (2013).

This observation counters current knowledge, which presents MIS 31 (1081-1062 ka) as the warmest interglacial during this period. It is generally referred to as the 'Super Interglacial', associated with maxima in obliquity, eccentricity and insolation (DeConto et al., 2012; Melles et al., 2012). However, this result is consistent with interpretations made at sites off the Iberian Peninsula. Indeed cores U1385 and U1387 show that MIS 31 is not associated with particularly high temperature conditions compared to those recorded at high latitudes (Voelker et al., 2015; Oliveira et al., 2017). Finally, in ODP site 976, MIS 31 is less marked than MIS 37 in terms of isotope values, pollen and foraminifera assemblages, and is closer to MIS 33 (1114-1104 ka) and MIS 35 (1190-1141 ka).

Concerning glacial phases, MIS 34 (1141-1114 ka) seems to be the most pronounced, with significant steppe expansion (~28%) and forest regression (10%). *Neogloboquadrina pachyderma* reached 40% and

https://doi.org/10.5194/egusphere-2026-1342
Preprint. Discussion started: 18 March 2026

reconstructions estimate an annual air temperature of ~9°C, which is corroborated by high $\delta^{18}O$ values of up to 1.62‰. However, these values remain very close to those observed during MIS 36 (1215-1190 ka). Reconstructed SSTs show colder values for MIS 36 (9.5°C) than MIS 34 (9.8°C), even though they remain within the same range of values. This slight difference can be explained by the combined presence of *Neogloboquadrina pachyderma* and the subpolar taxa *Turborotalita quinqueloba* in MIS 36, whereas the latter is almost absent in MIS 34.

A change in atmospheric and oceanographic conditions in the Western Mediterranean is recorded by clay mineralogy analyses. The illite/kaolinite (I/K) ratio is often used to demonstrate a shift in dust sources from North Africa. Currently, illite decreases from 60% of clay content in Northern Algeria to 30% in the Sahelian area (Paquet et al., 1984), whereas kaolinite, scarce in the northern Sahara, increases progressively southward and eastward and becomes dominant in the Sahel (Caquineau et al., 1998; Guerzoni et al., 1999; Bout-Roumazeilles et al., 2007; Stumpf et al., 2011). A high I/K ratio therefore suggests inputs preferentially from the Sahara, while lower values indicate a provenance associated with the Sahel. In ODP 976, the I/K ratio strongly increases after the transition between MIS 35 and 34 (around 1140 ka), reflecting a dominant Saharan origin for aeolian particles (Fig.8). This suggests the development of arid conditions with an enhanced supply of Saharan vs Sahelian origin at that time (Bout-Roumazeilles et al., 2007; Skonieczny et al., 2011).

While variations in the I/K ratio are commonly used to retrace aeolian supplies, the interpretation of the individual clay mineral as smectite is less direct and more complex. Indeed, smectite is ubiquitous in various types of environments, as it is easily transported over long-range distances due to its specific buoyancy characteristics. Smectite is a dominant component of suspended particulate material in the Alboran Sea (Pierce and Stanley, 1975; Grousset et al., 1988; Baringer and Price, 1999), especially within the Western Alboran Gyre (Bulian, 2022), resulting from the interaction between the smectite-rich entering surface Atlantic water, and smectite-rich Levantine Intermediate Water and Western Mediterranean Deep Water (Ambar and Howe, 1979; Bryden and Stommel, 1984; Millot, 2014). In that context, smectite variations in ODP 976 are interpreted as reflecting the oceanic advection of terrigenous material in the Alboran Sea, whereas the I/K ratio should only be used to retrace aeolian supply. A shift in the smectite signal is observed at ~1140ka, concomitant to the observed shift in the I/K ratio, suggesting a change in terrigenous advection and thus in the oceanic configuration in the Alboran Sea around 1140 ka.

In the Central Mediterranean, the vegetation signal from Montalbano Jonico shows extensive steppe developments during glacial periods and different interglacial periods compared to the western basin, more pronounced in MIS 31 and 35 than MIS 37 (Fig. 8.b). This shows the influence of the Atlantic mitigated forest development during the MIS 31 super interglacial period, compared to the Eastern Mediterranean. In the marine environment, the signal also differs from ODP site 976 with the dominance of *Turborotalita quinqueloba* and higher values for *Globigerinoides ruber* and lesser values for *Neogloboquadrina pachyderma* and *Neogloboquadrina incompta*. The central Mediterranean waters therefore appear warmer than in the western basin, but still relatively cool due to the presence of *Turborotalita quinqueloba*, which is consistent with a lesser influence of the input of cold Atlantic waters through the Gibraltar Strait. Throughout the period, *Turborotalita quinqueloba* variations appear to be partly linked to interglacial-glacial variations. At the end of MIS 35, it experienced a drastic decline (from 80 % to 20%). This cold-water taxon represents very productive waters and reflects the distribution of water masses and the stratification of the water column (Capotondi et al., 2004; Girone et al., 2013; Schiebel and Hemleben, 2017; Bazzicalupo et al., 2018). This major decline coincides with changes in the percentage of

https://doi.org/10.5194/egusphere-2026-1342
Preprint. Discussion started: 18 March 2026

smectite in the Alboran basin (Fig.8.a.b). However, this event is not found in the clay mineralogy from ODP Site 964 in the Ionian Sea (Zhao et al., 2016), nor further east at Site MD90-964 in the Levantine Basin (Zhao et al., 2011). This suggests that the change in marine circulation in the Alboran Sea is likely associated with Atlantic circulation and attenuates eastwards in the Mediterranean.

5.2. Late Early Pleistocene climate in the Southwest Mediterranean

Among the small number of continuous palynological sequences from the Early-Middle Pleistocene period in the Mediterranean, only two provide climate reconstruction data; Palominas site in southern Spain (Altolaguirre et al., 2020) with the Coexistence approach (CA) and Acigöl site in Türkiye (Robles et al, in revision), with a multi-method approach (CAM, MAT, WAPLS, RF and BRT). To discuss the climate of the Western Mediterranean Basin with a multi-site approach, additional pollen-based climate reconstructions were carried out using data from Monte San Giorgio and Palominas, following a multi-method approach (CAM, MAT, WAPLS, RF and BRT).

The three Western Mediterranean sites present consistent temperature variations (MAAT), which mirror the alternation of glacial and interglacial phases (Fig. 9). The MAT, WAPLS, BRT, and CAM methods show average annual temperatures of around 11 to 12°C for both marine sites (ODP site 976 and Monte San Giorgio) over the entire period, while the RF drops to an average of 10°C (Fig. 9.a.c.). In the continental sequence of Palominas, average temperature varies depending on the method used: 15°C for CA, 12°C for CAM, 10°C for MAT and BRT, 9.5°C for RF and 8°C for WAPLS (Fig.9.b). The lower values appear to be consistent with the altitude of the site, around 780 m above sea level. However, these values seem very cold for annual temperatures in this Southern Mediterranean region, where current values are around 16 to 19°C (Brun et al., 2022). The MAT method shows the greatest fluctuations over time across all sites. For precipitation (PANN), the signal from ODP site 976 mirrors the interglacial-glacial variations with large amplitudes for MAT and WAPLS (Fig. 9.a). The other two sites show wetter conditions for certain glacial phases: MIS 34 at Monte San Giorgio, except for CAM, and MIS 36 at Palominas (Fig. 9.b.c). In addition, MIS 35 appears drier at Palominas than at ODP 976 and Monte San Giorgio. MIS 34 appears quite marked at ODP site 976 and Monte San Giorgio with temperature decreases down to 9°C depending on the method. However, precipitation is reversed at Monte San Giorgio with more rainfall during this cold period. Even though this phase seems to be the most intense, it remains close to the conditions obtained for MIS 36, which are dry at Monte San Giorgio and ODP site 976, but wet at Palominas. This observation is consistent with current knowledge presenting MIS 34 as a very cold phase (Hodell et al., 2023; Margari et al., 2023), but we cannot exclude the possibility that conditions were less extreme in other Mediterranean areas.

CAM reconstruction shows higher precipitation and temperature fluctuations for Monte San Giorgio and Palominas than for ODP 976. Two hypotheses based on pollen data may explain this difference: i) forest diversity at the ODP 976 site is lower than at the other sites as the signal is almost exclusively composed of deciduous *Quercus*; ii) the slightly higher presence of relict taxa, among them *Tsuga*, *Zelkova* or *Cathaya*. The deciduous *Quercus* pollen type encompasses a large number of species that develop within a very wide temperature range (MAAT: 5 and 23°C; Fauquette 1998), which does not allow for effective constraints on climate reconstruction. The other temperate deciduous forest taxa, which are present within narrower temperature ranges, are not present in sufficient quantities to exceed the presence and abundance thresholds, and therefore to constrain the climate estimate. For the other two sites, *Quercus* also dominates the assemblage, but other taxa are sufficiently represented

https://doi.org/10.5194/egusphere-2026-1342
Preprint. Discussion started: 18 March 2026

to constrain the model, such as *Ulmus* or *Ostrya* and *Celtis* for the Spanish site, and *Carpinus* for the Italian site. Monte San Giorgio also presents sufficient quantities of Arecaceae to better constrain the reconstruction.

The methods applied to the Palominas dataset (CAM, MAT, BRT, RF, and WAPLS) are consistently colder than the results provided by the Coexistence Approach (CA) (Altolaguirre et al., 2020). They rely on different modern databases: PALEOFLORA for the CA (www.paleoflora.de), the database of modern pollen spectra used by Fauquette et al. (1998) for the CAM and the Eurasian and Mediterranean Current Surface Sample Database (EAPDB; Peyron et al., 1998, 2011, 2013) for the other methods. The difference between the CAM and CA is all the more striking since they are based on similar concept and parameterization choices (i.e., the removal of taxa present only once, Altolaguirre et al., 2020).

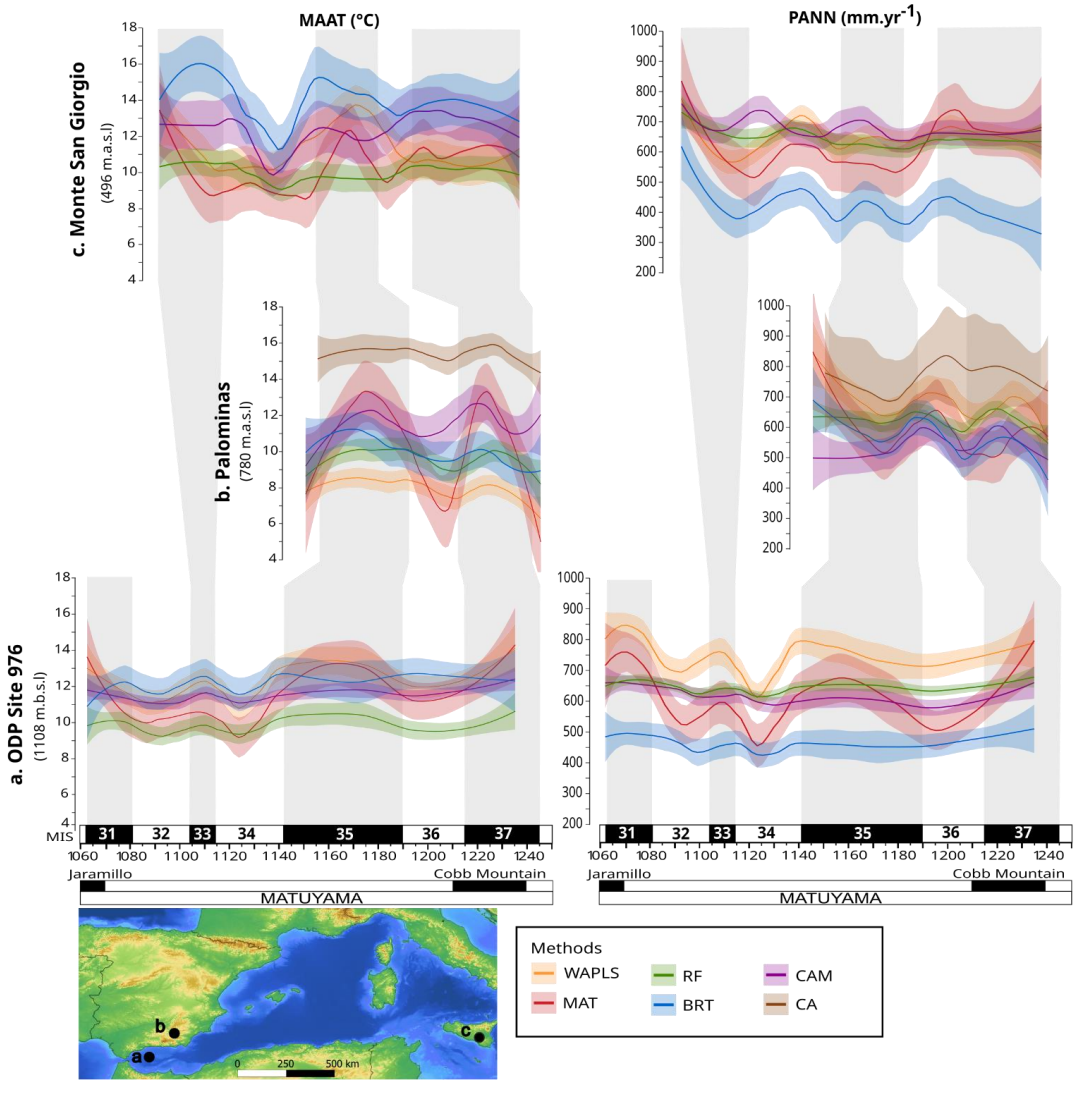

Figure 9. Mean Annual Air Temperature (MAAT) and Annual Precipitation (PANN) reconstructions of three sites in the Western Mediterranean basin between 36 and 38°N: ODP site 976, Palominas and Monte San Giorgio. Five methods were used: Weighted Averaging Partials Least Square (WAPLS), Modern Analog Technique (MAT), Random Forest

https://doi.org/10.5194/egusphere-2026-1342
Preprint. Discussion started: 18 March 2026

(RF), Boosted Regression Tree (BRT) and Climatic Amplitude Method (CAM). For Palominas, the Coexistence Approach (CA) method was performed by Altolaguirre et al (2020). m.b.s.l: metres below sea level; m.a.s.l: metres above sea level.

5.3. Comparison with climate reconstruction from archaeological/palaeontological sites in South-western Spain

In southern Spain, archaeological faunal data is an additional proxy for climate reconstructions and comparisons with pollen-based climate reconstructions from Palominas and ODP 976. The faunal assemblages come from archaeological sites (Fuente Nueva 3, Barranco Leon and Cueva Victoria) and palaeontological sites (Quibas and El Chaparral) (Fig. 10). Faunal-based climate reconstructions follow three different methods in terms of concepts and types of fauna. All these sites have higher temperature estimates (Fig. 10) than the temperature reconstructions based on pollen assemblages (Fig. 9). Only the results of the Coexistence Approach from Palominas pollen data (Fig. 9) are in the same range of values (15.5°C). On the other hand, pollen-based reconstructions of precipitation are more consistent with results from faunal data (Fig. 10). The WAPLS values in ODP 976 and Palominas (~750 and ~700 mm/year) are close to those reconstructed at Fuente Nueva (738-753 mm/year; Agustí et al. (2009); Blain et al. (2011, 2016)), Barranco Léon (732-741 mm/year; Agustí et al. (2009); Blain et al. (2011)), Quibas (723 mm/year; Agustí et al. (2009)) and Cueva Victoria (716 mm/year; Agustí et al. (2009)). BRT values (~475 mm/year) in ODP 976 are close to the lowest reconstructed precipitation values at Quibas (417 mm/year; Hernández Fernández et al. (2007)). This probably suggests that climate and vegetation in the southern Mediterranean region were more strongly influenced by, and sensitive to, variations in rainfall and drought than temperatures. Underestimations of temperatures using pollen-based reconstruction methods raise questions about the methodology, the modern databases used, the functioning of each method, and the application of these methods to marine pollen records and to the ancient Quaternary period (except for CAM which was developed for Neogene and Early Quaternary climate reconstruction). In the case of the two marine sites ODP 976 and Monte San Giorgio, temperatures appear to be underestimated. However, this same trend is observed at the continental site of Palominas. Unlike faunal data, ODP 976 records plants in the Alboran Sea from a large area stretching from the coasts to the mountains of both Morocco and southern Spain. The reconstructed climate is therefore an average climate over a large geographical area and not a local one.

https://doi.org/10.5194/egusphere-2026-1342
Preprint. Discussion started: 18 March 2026

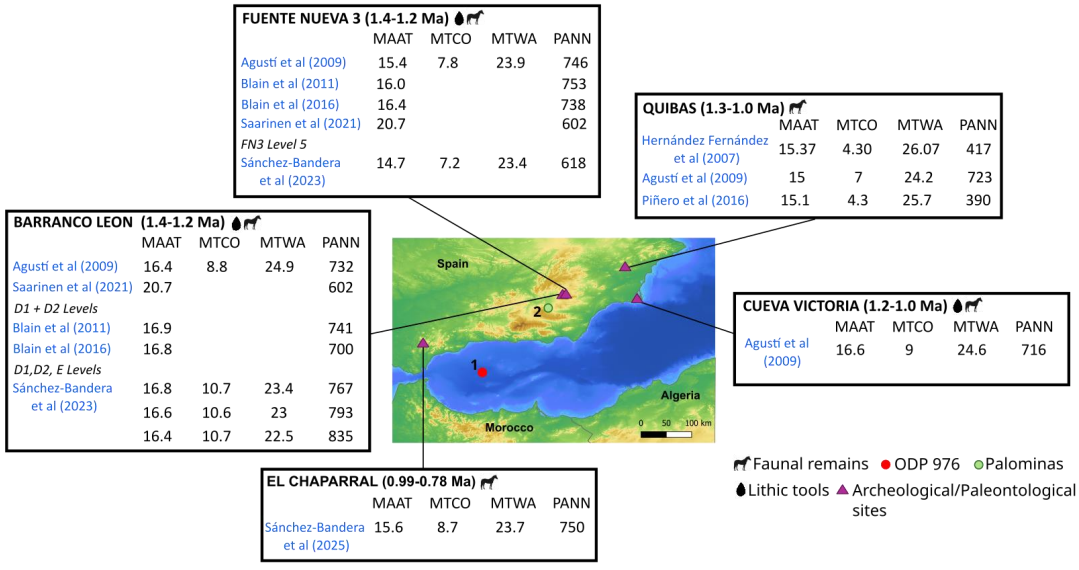

Figure 10. Climate reconstruction based on faunal assemblages from archaeological and palaeontological sites in south-eastern Spain. Palaeontological sites are represented by the image of a horse, and archaeological sites are represented by a stone tool. MAAT, MTCO and MTWA are in degrees and PANN in mm per year.

Conclusion

This high-resolution study of the ODP 976 site provides multiproxy reconstructions of climate change in the South-western Mediterranean at the end of the Early Pleistocene. The sequence continuously documents marine and continental environments during the EMPT, when climate cycles began to lengthen from 41 kyr to 100 kyr. This multiproxy approach highlights the synchronicity between the continental and marine response to glacial-interglacial cycles in the Western Mediterranean between MIS 37 and MIS 31 (~1235-1062 ka). Comparisons with other sequences from the Central and Western Mediterranean show major differences between the Iberian Peninsula and southern Italy. Results highlight a marked climatic gradient between the Western and Central Mediterranean during MIS 31, constraining forest development under the influence of the Atlantic climate system, compared to southern Italy, which was less affected by this dynamic. Clay mineralogy shows an abrupt change in smectite and I/K signals, reflecting atmospheric and marine conditions in the Alboran Sea around 1140 ka, i.e., at the transition between MIS 35 and 34. Multi-method climate reconstructions based on foraminifera and pollen assemblages show variations in temperature and precipitation mirroring climate cycles. However, some glacial periods appear wetter than some interglacial periods, depending on the method used. MIS 34 reconstructions appear more pronounced in terms of temperature and precipitation, compared to other glacial phases. In contrast to CA reconstructions, CAM, MAT, WAPLS, RF and BRT pollen-based reconstructions systematically show colder temperatures than those based on faunal assemblages from palaeontological and archaeological sites in southern Spain, which could be explained by local *vs* regional climate reconstruction. On the other hand, precipitation reconstruction seems more consistent for the two types of archives, suggesting that vegetation

https://doi.org/10.5194/egusphere-2026-1342
Preprint. Discussion started: 18 March 2026

changes are driven more by precipitation than temperature fluctuations in this part of the Southern Mediterranean. These results enhance our understanding of the environmental changes that occurred in the Western Mediterranean during the period between MIS 37-31, providing land-sea information. This type of research must now be extended to the entire EMPT in order to better understand the climate changes that took place at a time of major modification of the Earth's climate system, and to comprehend the environmental context in which the first hominins settled in Western Europe.

Competing interests

One of the authors (O. Peyron) is a member of the editorial board of Climate of the Past. The other authors declare that they have no competing interests.

Data availability

Data will be made available upon request to the corresponding author.

Author contribution

MC, VL, NCN, OP, SF designed the project. MC performed the palynological analyses and MF and JL the foraminifera assemblages. PR and MF conducted the isotope analyses used for the age model and VBR and MD the clay mineralogy analysis. LD conducted all the palynological HF attack treatment. MC, MR, OP, and SF performed the climate reconstruction on pollen data. MF applied the SST reconstruction method to foraminifera assemblages. SJ, YA, JPS gave permission to use their data and contributed to the interpretation of results. All the co-authors participated in writing this manuscript and in the discussion of results.

Acknowledegments

We are grateful to the ERC LATEUROPE project (n°101052653), the Centre National de la Recherche Scientifique (CNRS) and the Museum national d'Histoire naturelle (MNHN) for their financial support. We thank the PANOPLY analytical platform at LSCE for facilities for carrying out isotopic measurements and the study of the foraminifera assemblages, and the Ocean Drilling Program (ODP) for making available material from the core ODP leg 161 site 976. We thank Amandine Viala for providing us with her code to use the PERMANOVA non-parametric test. We would also like to thank Angela Girone for sharing and giving us permission to use her data. This is an ISEM publication n° XXXX.

Financial support

This project was financially supported by the ERC LATEUROPE project (n°101052653), by the Centre National de la Recherche Scientifique (CNRS) and by the Museum National d'Histoire Naturelle (MNHN)

References

Agustí, J., Blain, H.-A., Cuenca-Bescós, G., and Bailon, S.: Climate forcing of first hominid dispersal in Western Europe, Journal of Human Evolution, 57, 815–821, https://doi.org/10.1016/j.jhevol.2009.06.005, 2009.

https://doi.org/10.5194/egusphere-2026-1342
Preprint. Discussion started: 18 March 2026

Altolaguirre, Y., Bruch, A. A., and Gibert, L.: A long Early Pleistocene pollen record from Baza Basin (SE Spain): Major contributions to the palaeoclimate and palaeovegetation of Southern Europe, Quaternary Science Reviews, 231, 106199, https://doi.org/10.1016/j.quascirev.2020.106199, 2020.

Ambar, I. and Howe, M. R.: Observations of the Mediterranean outflow—I mixing in the Mediterranean outflow, Deep Sea Research Part A. Oceanographic Research Papers, 26, 535–554, https://doi.org/10.1016/0198-0149(79)90095-5, 1979.

Bahr, A., Kaboth, S., Hodell, D., Zeeden, C., Fiebig, J., and Friedrich, O.: Oceanic heat pulses fueling moisture transport towards continental Europe across the mid-Pleistocene transition, Quaternary Science Reviews, 179, 48–58, https://doi.org/10.1016/j.quascirev.2017.11.009, 2018.

Bahr, A., Catunda, M. C. A., and Friedrich, O.: The first appearance of Glacial North Atlantic Intermediate Water (GNAIW) during the Mid-Pleistocene transition, Global and Planetary Change, 218, 103977, https://doi.org/10.1016/j.gloplacha.2022.103977, 2022.

Baringer, M. O. and Price, J. F.: A review of the physical oceanography of the Mediterranean outflow, Marine Geology, 155, 63–82, https://doi.org/10.1016/S0025-3227(98)00141-8, 1999.

Barker, S., Starr, A., Conn, S., Lordsmith, S., Owen, L., Nederbragt, A., Hemming, S., Hall, I., and Levay, L.: Persistent influence of precession on northern ice sheet variability since the early Pleistocene, Science, 376, 961–967, https://doi.org/10.1126/science.abm4033, 2022.

Bazzicalupo, P., Maiorano, P., Girone, A., Marino, M., Combourieu-Nebout, N., and Incarbona, A.: High-frequency climate fluctuations over the last deglaciation in the Alboran Sea, Western Mediterranean: Evidence from calcareous plankton assemblages, Palaeogeography, Palaeoclimatology, Palaeoecology, 506, 226–241, https://doi.org/10.1016/j.palaeo.2018.06.042, 2018.

Beck, H. E., McVicar, T. R., Vergopolan, N., Berg, A., Lutsko, N. J., Dufour, A., Zeng, Z., Jiang, X., Van Dijk, A. I. J. M., and Miralles, D. G.: High-resolution (1 km) Köppen-Geiger maps for 1901–2099 based on constrained CMIP6 projections, Sci Data, 10, 724, https://doi.org/10.1038/s41597-023-02549-6, 2023.

Benabid, A.: Les écosystèmes forestiers, préforestiers et presteppiques du Maroc : diversité, répartition biogéographique et problèmes posés par leur aménagement, Forêt Méditerranéenne, VII, 53–64, 1985.

Berends, C. J., Köhler, P., Lourens, L. J., and van de Wal, R. S. W.: On the Cause of the Mid-Pleistocene Transition, Reviews of Geophysics, 59, e2020RG000727, https://doi.org/10.1029/2020RG000727, 2021.

Blain, H.-A., Bailon, S., and Agustí, J.: Anurans and squamate reptiles from the latest early Pleistocene of Almenara-Casablanca-3 (Castellón, East of Spain). Systematic, climatic and environmental considerations, 2007.

Blain, H.-A., Bailon, S., Cuenca-Bescós, G., Arsuaga, J. L., Bermúdez De Castro, J. M., and Carbonell, E.: Long-term climate record inferred from early-middle Pleistocene amphibian and squamate reptile assemblages at the Gran Dolina Cave, Atapuerca, Spain, Journal of Human Evolution, 56, 55–65, https://doi.org/10.1016/j.jhevol.2008.08.020, 2009.

Blain, H.-A., Bailon, S., Agustí, J., Martínez-Navarro, B., and Toro, I.: Paleoenvironmental and paleoclimatic proxies to the Early Pleistocene hominids of Barranco León D and Fuente Nueva 3 (Granada, Spain) by means of their amphibian and reptile assemblages, Quaternary International, 243, 44–53, https://doi.org/10.1016/j.quaint.2010.12.031, 2011.

Blain, H.-A., Lozano-Fernández, I., Agustí, J., Bailon, S., Menéndez Granda, L., Espígares Ortiz, M. P., Ros-Montoya, S., Jiménez Arenas, J. M., Toro-Moyano, I., Martínez-Navarro, B., and Sala, R.: Refining upon the

https://doi.org/10.5194/egusphere-2026-1342
Preprint. Discussion started: 18 March 2026

climatic background of the Early Pleistocene hominid settlement in western Europe: Barranco León and Fuente Nueva-3 (Guadix-Baza Basin, SE Spain), Quaternary Science Reviews, 144, 132–144, https://doi.org/10.1016/j.quascirev.2016.05.020, 2016.

Bout-Roumazeilles, V., Cortijo, E., Labeyrie, L., and Debrabant, P.: Clay mineral evidence of nepheloid layer contributions to the Heinrich layers in the northwest Atlantic, Palaeogeography, Palaeoclimatology, Palaeoecology, 146, 211–228, https://doi.org/10.1016/S0031-0182(98)00137-0, 1999.

Bout-Roumazeilles, V., Combourieu Nebout, N., Peyron, O., Cortijo, E., Landais, A., and Masson-Delmotte, V.: Connection between South Mediterranean climate and North African atmospheric circulation during the last 50,000yrBP North Atlantic cold events, Quaternary Science Reviews, 26, 3197–3215, https://doi.org/10.1016/j.quascirev.2007.07.015, 2007.

Breiman, L.: Random Forests, Machine Learning, 45, 5–32, https://doi.org/10.1023/A:1010933404324, 2001.

Breiman, L., Cutler, A., Liaw, A., and Wiener, M.: Package 'randomForest,' , 4.7–1.2, 2024.

Brown, G. and Brindley, G. W.: X-ray Diffraction Procedures for Clay Mineral Identification, in: Crystal Structures of Clay Minerals and their X-Ray Identification, edited by: Brown, G. and Brindley, G. W., Mineralogical Society, London, 305–359, 1980.

Brun, P., Zimmermann, N. E., Hari, C., and Karger, D. N.: CHELSA-BIOCLIM+ A novel set of global climate-related predictors at kilometre-resolution, https://www.doi.org/10.16904/envidat.332, 2022.

Bryden, H. L. and Stommel, H. M.: Limiting processes that determine basic features of the circulation in the Mediterranean Sea, Oceanologia acta, 7, 289–296, 1984.

Bulian, F.: The late Miocene – early Pliocene offshore onshore sedimentary records in the vicinity of Gibraltar, Universidad de Salamanca, 2022.

Capotondi, L., Soroldoni, E., and Principato, M. S.: Late Quaternary planktonic foraminiferal distributions: problems related to size fraction, Proceedings of the First Italian Meeting on Environmental, 2004.

Caquineau, S., Gaudichet, A., Gomes, L., Magonthier, M.-C., and Chatenet, B.: Saharan dust: Clay ratio as a relevant tracer to assess the origin of soil-derived aerosols, Geophysical Research Letters, 25, 983–986, https://doi.org/10.1029/98GL00569, 1998.

Carbonell, E., Bermúdez de Castro, J. M., Parés, J. M., Pérez-González, A., Cuenca-Bescós, G., Ollé, A., Mosquera, M., Huguet, R., van der Made, J., Rosas, A., Sala, R., Vallverdú, J., García, N., Granger, D. E., Martinón-Torres, M., Rodríguez, X. P., Stock, G. M., Vergès, J. M., Allué, E., Burjachs, F., Cáceres, I., Canals, A., Benito, A., Díez, C., Lozano, M., Mateos, A., Navazo, M., Rodríguez, J., Rosell, J., and Arsuaga, J. L.: The first hominin of Europe, Nature, 452, 465–469, https://doi.org/10.1038/nature06815, 2008.

Catrain, M., Combourieu Nebout, N., Lebreton, V., Fauquette, S., Peyron, O., Fries, M., Richard, P., Dubost, L., Joannin, S., Suc, J.-P., Paquier Comas, E., Lepelletier, J., and Moncel, M.-H.: Vegetation and climate dynamics in the south-western mediterranean during MIS 37–31 (~1.25 - ~1. 06 Ma): Insights from the marine core ODP site 976, Quaternary Science Reviews, 369, https://doi.org/10.1016/j.quascirev.2025.109635, 2025.

Chalk, T. B., Hain, M. P., Foster, G. L., Rohling, E. J., Sexton, P. F., Hendry, K. R., Badger, M. P. S., Cherry, S. G., Hasenfratz, A. P., Haug, G. H., Jaccard, S. L., Martínez-García, A., Pälike, H., Pancost, R. D., and Wilson, P. A.: Causes of ice age intensification across the Mid-Pleistocene Transition, Proceedings of the National Academy of Sciences of the United States of America, 114, 13114–13119, https://doi.org/10.1073/pnas.1702143114, 2017.

https://doi.org/10.5194/egusphere-2026-1342
Preprint. Discussion started: 18 March 2026

Charton, L., Combourieu-Nebout, N., Bertini, A., Lebreton, V., Peyron, O., Robles, M., Sassoon, D., and Moncel, M.-H.: Vegetation and climate changes during the Middle to Upper Palaeolithic transition in the southwestern Mediterranean: What happened to the last Neanderthals during Heinrich stadial 4?, Quaternary Science Reviews, 359, 109345, https://doi.org/10.1016/j.quascirev.2025.109345, 2025.

Chevalier, M., Davis, B. A. S., Heiri, O., Seppä, H., Chase, B. M., Gajewski, K., Lacourse, T., Telford, R. J., Finsinger, W., Guiot, J., Kühl, N., Maezumi, S. Y., Tipton, J. R., Carter, V. A., Brussel, T., Phelps, L. N., Dawson, A., Zanon, M., Vallé, F., Nolan, C., Mauri, A., de Vernal, A., Izumi, K., Holmström, L., Marsicek, J., Goring, S., Sommer, P. S., Chaput, M., and Kupriyanov, D.: Pollen-based climate reconstruction techniques for late Quaternary studies, Earth-Science Reviews, 210, 103384, https://doi.org/10.1016/j.earscirev.2020.103384, 2020.

Clark, P. U., Archer, D., Pollard, D., Blum, J. D., Rial, J. A., Brovkin, V., Mix, A. C., Pisias, N. G., and Roy, M.: The middle Pleistocene transition: characteristics, mechanisms, and implications for long-term changes in atmospheric pCO2, Quaternary Science Reviews, 25, 3150–3184, https://doi.org/10.1016/j.quascirev.2006.07.008, 2006.

Cucart-Mora, C., Lombao, D., Pineda, A., Boemke, B., Mecozzi, B., and Moncel, M.-H.: The First Occupations of Western Europe: Dispersals and Population Dynamics in the Early to Middle Pleistocene, J Archaeol Method Theory, 33, 19, https://doi.org/10.1007/s10816-025-09752-2, 2026.

Daget, P.: Le bioclimat mediterraneen: Caracteres generaux, modes de caracterisation, Vegetatio, 34, 1–20, https://doi.org/10.1007/BF00119883, 1977.

Davis, B. A. S., Chevalier, M., Sommer, P., Carter, V. A., Finsinger, W., Mauri, A., Phelps, L. N., Zanon, M., Abegglen, R., Åkesson, C. M., Alba-Sánchez, F., Anderson, R. S., Antipina, T. G., Atanassova, J. R., Beer, R., Belyanina, N. I., Blyakharchuk, T. A., Borisova, O. K., Bozilova, E., Bukreeva, G., Bunting, M. J., Clò, E., Colombaroli, D., Combourieu-Nebout, N., Desprat, S., Di Rita, F., Djamali, M., Edwards, K. J., Fall, P. L., Feurdean, A., Fletcher, W., Florenzano, A., Furlanetto, G., Gaceur, E., Galimov, A. T., Gałka, M., García-Moreiras, I., Giesecke, T., Grindean, R., Guido, M. A., Gvozdeva, I. G., Herzschuh, U., Hjelle, K. L., Ivanov, S., Jahns, S., Jankovska, V., Jiménez-Moreno, G., Karpińska-Kołaczek, M., Kitaba, I., Kołaczek, P., Lapteva, E. G., Latałowa, M., Lebreton, V., Leroy, S., Leydet, M., Lopatina, D. A., López-Sáez, J. A., Lotter, A. F., Magri, D., Marinova, E., Matthias, I., Mavridou, A., Mercuri, A. M., Mesa-Fernández, J. M., Mikishin, Y. A., Milecka, K., Montanari, C., Morales-Molino, C., Mrotzek, A., Muñoz Sobrino, C., Naidina, O. D., Nakagawa, T., Nielsen, A. B., Novenko, E. Y., Panajiotidis, S., Panova, N. K., Papadopoulou, M., Pardoe, H. S., Pędziszewska, A., Petrenko, T. I., Ramos-Román, M. J., Ravazzi, C., Rösch, M., Ryabogina, N., Sabariego Ruiz, S., Salonen, J. S., Sapelko, T. V., Schofield, J. E., Seppä, H., Shumilovskikh, L., Stivrins, N., Stojakowits, P., Svobodova Svitavska, H., Święta-Musznicka, J., Tantau, I., Tinner, W., Tobolski, K., Tonkov, S., Tsakiridou, M., et al.: The Eurasian Modern Pollen Database (EMPD), version 2, Earth System Science Data, 12, 2423–2445, https://doi.org/10.5194/essd-12-2423-2020, 2020.

De'ath, G.: Boosted Trees for Ecological Modeling and Prediction, Ecology, 88, 243–251, https://doi.org/10.1890/0012-9658(2007)88%255B243:BTFEMA%255D2.0.CO;2, 2007.

DeConto, R. M., Pollard, D., and Kowalewski, D.: Modeling Antarctic ice sheet and climate variations during Marine Isotope Stage 31, Global and Planetary Change, 88–89, 45–52, https://doi.org/10.1016/j.gloplacha.2012.03.003, 2012.

https://doi.org/10.5194/egusphere-2026-1342
Preprint. Discussion started: 18 March 2026

Donders, T., Panagiotopoulos, K., Koutsodendris, A., Bertini, A., Mercuri, A. M., Masi, A., Combourieu-Nebout, N., Joannin, S., Kouli, K., Kousis, I., Peyron, O., Torri, P., Florenzano, A., Francke, A., Wagner, B., and Sadori, L.: 1.36 million years of Mediterranean forest refugium dynamics in response to glacial–interglacial cycle strength, Proceedings of the National Academy of Sciences, 118, e2026111118, https://doi.org/10.1073/pnas.2026111118, 2021.

Dugerdil, L., Joannin, S., Peyron, O., Jouffroy-Bapicot, I., Vannière, B., Boldgiv, B., Unkelbach, J., Behling, H., and Ménot, G.: Climate reconstructions based on GDGT and pollen surface datasets from Mongolia and Baikal area: calibrations and applicability to extremely cold–dry environments over the Late Holocene, Clim. Past, 17, 1199–1226, https://doi.org/10.5194/cp-17-1199-2021, 2021.

Duval, M., Arnold, L. J., Bahain, J.-J., Parés, J. M., Demuro, M., Falguères, C., Shao, Q., Voinchet, P., Arnaud, J., Berto, C., Berruti, G. L. F., Daffara, S., Sala, B., and Arzarello, M.: Re-examining the earliest evidence of human presence in western Europe: New dating results from Pirro Nord (Italy), Quaternary Geochronology, 82, 101519, https://doi.org/10.1016/j.quageo.2024.101519, 2024.

Elenga, H., Peyron, O., Bonnefille, R., Jolly, D., Cheddadi, R., Guiot, J., Andrieu, V., Bottema, S., Buchet, G., De Beaulieu, J. -L., Hamilton, A. C., Maley, J., Marchant, R., Perez-Obiol, R., Reille, M., Riollet, G., Scott, L., Straka, H., Taylor, D., Van Campo, E., Vincens, A., Laarif, F., and Jonson, H.: Pollen-based biome reconstruction for southern Europe and Africa 18,000 yr BP, Journal of Biogeography, 27, 621–634, https://doi.org/10.1046/j.1365-2699.2000.00430.x, 2000.

Elith, J., Leathwick, J. R., and Hastie, T.: A working guide to boosted regression trees, Journal of Animal Ecology, 77, 802–813, https://doi.org/10.1111/j.1365-2656.2008.01390.x, 2008.

Fabres, J., Calafat, A., Sanchez-Vidal, A., Canals, M., and Heussner, S.: Composition and spatio-temporal variability of particle fluxes in the Western Alboran Gyre, Mediterranean Sea, Journal of Marine Systems, 33–34, 431–456, https://doi.org/10.1016/S0924-7963(02)00070-2, 2002.

Fauquette, S., Guiot, J., and Suc, J.-P.: A method for climatic reconstruction of the Mediterranean Pliocene using pollen data, Palaeogeography, Palaeoclimatology, Palaeoecology, 144, 183–201, https://doi.org/10.1016/S0031-0182(98)00083-2, 1998.

Girone, A., Capotondi, L., Ciaranfi, N., Di Leo, P., Lirer, F., Maiorano, P., Marino, M., Pelosi, N., and Pulice, I.: Paleoenvironmental changes at the lower Pleistocene Montalbano Jonico section (southern Italy): Global versus regional signals, Palaeogeography, Palaeoclimatology, Palaeoecology, 371, 62–79, https://doi.org/10.1016/j.palaeo.2012.12.017, 2013.

Grimm, E.: Tilia and Tiliagrah, Illinois State Museum, Springfield., 1991.

Grousset, F. E., Joron, J. L., Biscaye, P. E., Latouche, C., Treuil, M., Maillet, N., Faugères, J. C., and Gonthier, E.: Mediterranean outflow through the Strait of Gibraltar since 18,000 Years B.P.: Mineralogical and geochemical arguments, Geo-Marine Letters, 8, 25–34, https://doi.org/10.1007/BF02238003, 1988.

Guerzoni, S., Molinaroli, E., Rossini, P., Rampazzo, G., Quarantotto, G., De Falco, G., and Cristini, S.: Role of desert aerosol in metal fluxes in the Mediterranean area, Chemosphere, 39, 229–246, https://doi.org/10.1016/S0045-6535(99)00105-8, 1999.

Guijarro, J. A., Conde, J., Campins, J., Orro, M. L., and Picornell, M. Á.: Atlas de clima marítimo (0-52ºN, 35ºW-12ºE; 1981-2010), Agencia Estatal de Meteorología, https://doi.org/10.31978/281-15-028-8, 2015.

https://doi.org/10.5194/egusphere-2026-1342
Preprint. Discussion started: 18 March 2026

754 Guiot, J.: Methodology of palaeoclimatic reconstruction from pollen in France: Palaeogeography,
755 Palaeogeography, Palaeoclimatology, Palaeoecology, 80, 49–69, https://doi.org/10.1016/0031-0182(90)90033-4,
756 1990.
757 Guo, Q., Li, B., Voelker, A. H. L., and Kim, J.-K.: Mediterranean Outflow Water dynamics across the middle
758 Pleistocene transition based on a 1.3 million-year benthic foraminiferal record off the Portuguese margin,
759 Quaternary Science Reviews, 247, 106567, https://doi.org/10.1016/j.quascirev.2020.106567, 2020.
760 Head, M. J. and Gibbard, P. L.: Early–Middle Pleistocene transitions: Linking terrestrial and marine realms,
761 Quaternary International, 389, 7–46, https://doi.org/10.1016/j.quaint.2015.09.042, 2015.
762 Herbert, T. D.: The Mid-Pleistocene Climate Transition, Annual Review of Earth and Planetary Sciences, 51, 389–
763 418, https://doi.org/10.1146/annurev-earth-032320-104209, 2023.
764 Hijmans, R. J., Phillips, S., Leathwick, J., and Elith, J.: Package 'dismo,' , 1.3-16, 2024.
765 Hodell, D. A., Crowhurst, S. J., Lourens, L., Margari, V., Nicolson, J., Rolfe, J. E., Skinner, L. C., Thomas, N. C.,
766 Tzedakis, P. C., Mleneck-Vautravers, M. J., and Wolff, E. W.: A 1.5-million-year record of orbital and millennial
767 climate variability in the North Atlantic, Climate of the Past, 19, 607–636, https://doi.org/10.5194/cp-19-607-
768 2023, 2023.
769 Joannin, S., Ciaranfi, N., and Stefanelli, S.: Vegetation changes during the late Early Pleistocene at Montalbano
770 Jonico (Province of Matera, southern Italy) based on pollen analysis, Palaeogeography, Palaeoclimatology,
771 Palaeoecology, 270, 92–101, https://doi.org/10.1016/j.palaeo.2008.08.017, 2008.
772 Joannin, S., Bassinot, F., Nebout, N. C., Peyron, O., and Beaudouin, C.: Vegetation response to obliquity and
773 precession forcing during the Mid-Pleistocene Transition in Western Mediterranean region (ODP site 976),
774 Quaternary Science Reviews, 30, 280–297, https://doi.org/10.1016/j.quascirev.2010.11.009, 2011.
775 Juggins, S.: Package 'rioja,' , 1.0-7, 2024.
776 Köppen, W.: Das geographische System der Klimate, in: Handbuch der Klimatologie, vol. I, edited by: Köppen,
777 W. and Geiger, R., Verlag von Gebrüder Borntl'aeger, Berlin, 44, 1936.
778 Leblanc, M.: Étude des périodes humides Africaines enregistrées au cours des deux derniers cycles climatiques à
779 partir de la caractérisation de poussières Sahariennes déposées en Méditerranée Occidentale et dans l'océan
780 Atlantique Tropical Nord-Est, Université Paris-Saclay, 2022.
781 Lisiecki, L. E. and Raymo, M. E.: A Pliocene-Pleistocene stack of 57 globally distributed benthic δ18O records,
782 Paleoceanography, 20, https://doi.org/10.1029/2004PA001071, 2005.
783 Macías, D., Bruno, M., Echevarría, F., Vázquez, A., and García, C. M.: Meteorologically-induced mesoscale
784 variability of the North-western Alboran Sea (southern Spain) and related biological patterns, Estuarine, Coastal
785 and Shelf Science, 78, 250–266, https://doi.org/10.1016/j.ecss.2007.12.008, 2008.
786 Magri, D., Di Rita, F., Aranbarri, J., Fletcher, W., and González-Sampériz, P.: Quaternary disappearance of tree
787 taxa from Southern Europe: Timing and trends, Quaternary Science Reviews, 163, 23–55,
788 https://doi.org/10.1016/j.quascirev.2017.02.014, 2017.
789 Margari, V., Hodell, D. A., Parfitt, S. A., Ashton, N. M., Grimalt, J. O., Kim, H., Yun, K.-S., Gibbard, P. L.,
790 Stringer, C. B., Timmermann, A., and Tzedakis, P. C.: Extreme glacial cooling likely led to hominin depopulation
791 of Europe in the Early Pleistocene, Science, 381, 693–699, https://doi.org/10.1126/science.adf4445, 2023.
792 Marquina-Blasco, R., Sánchez-Bandera, C., López-García, J. M., Martínez-Ortí, A., Sevilla, P., Ruiz-Sánchez, F.
793 J., and Blain, H.-A.: Palaeoecological characterization of the Pliocene-Pleistocene transition on the Mediterranean

https://doi.org/10.5194/egusphere-2026-1342
Preprint. Discussion started: 18 March 2026

littoral area: Almenara-Casablanca (Castellón, eastern Spain), Quaternary Science Reviews, 352, 109154, https://doi.org/10.1016/j.quascirev.2024.109154, 2025.

Martínez-Botí, M. A., Foster, G. L., Chalk, T. B., Rohling, E. J., Sexton, P. F., Lunt, D. J., Pancost, R. D., Badger, M. P. S., and Schmidt, D. N.: Plio-Pleistocene climate sensitivity evaluated using high-resolution CO2 records, Nature, 518, 49–54, https://doi.org/10.1038/nature14145, 2015.

Maslin, M. A. and Brierley, C. M.: The role of orbital forcing in the Early Middle Pleistocene Transition, Quaternary International, 47–55, http://dx.doi.org/10.1016/j.quaint.2015.01.047, 2015.

Médail, F.: Plant Biogeography and Vegetation Patterns of the Mediterranean Islands, Bot. Rev., 88, 63–129, https://doi.org/10.1007/s12229-021-09245-3, 2022.

Melles, M., Brigham-Grette, J., Minyuk, P. S., Nowaczyk, N. R., Wennrich, V., DeConto, R. M., Anderson, P. M., Andreev, A. A., Coletti, A., Cook, T. L., Haltia-Hovi, E., Kukkonen, M., Lozhkin, A. V., Rosén, P., Tarasov, P., Vogel, H., and Wagner, B.: 2.8 Million Years of Arctic Climate Change from Lake El'gygytgyn, NE Russia, Science, 337, 315–320, https://doi.org/10.1126/science.1222135, 2012.

Millot, C.: Heterogeneities of in- and out-flows in the Mediterranean Sea, Progress in Oceanography, 120, 254–278, https://doi.org/10.1016/j.pocean.2013.09.007, 2014.

Moreno, A., Cacho, I., Canals, M., Grimalt, J. O., Sánchez-Goñi, M. F., Shackleton, N., and Sierro, F. J.: Links between marine and atmospheric processes oscillating on a millennial time-scale. A multi-proxy study of the last 50,000yr from the Alboran Sea (Western Mediterranean Sea), Quaternary Science Reviews, 24, 1623–1636, https://doi.org/10.1016/j.quascirev.2004.06.018, 2005.

Moyano, I. T., Barsky, D., Cauche, D., Celiberti, V., Grégoire, S., Lebegue, F., Moncel, M. H., and De Lumley, H.: The archaic stone tool industry from Barranco León and Fuente Nueva 3, (Orce, Spain): Evidence of the earliest hominin presence in southern Europe, Quaternary International, 243, 80–91, https://doi.org/10.1016/j.quaint.2010.12.011, 2011.

Oliveira, D., Sánchez Goñi, M. F., Naughton, F., Polanco-Martínez, J. M., Jimenez-Espejo, F. J., Grimalt, J. O., Martrat, B., Voelker, A. H. L., Trigo, R., Hodell, D., Abrantes, F., and Desprat, S.: Unexpected weak seasonal climate in the western Mediterranean region during MIS 31, a high-insolation forced interglacial, Quaternary Science Reviews, 161, 1–17, https://doi.org/10.1016/j.quascirev.2017.02.013, 2017.

d'Oliveira, L., Dugerdil, L., Ménot, G., Evin, A., Muller, S. D., Ansanay-Alex, S., Azuara, J., Bonnet, C., Bremond, L., Shah, M., and Peyron, O.: Reconstructing 15 000 years of southern France temperatures from coupled pollen and molecular (branched glycerol dialkyl glycerol tetraether) markers (Canroute, Massif Central), Climate of the Past, 19, 2127–2156, https://doi.org/10.5194/cp-19-2127-2023, 2023.

d'Oliveira, L., Joannin, S., Ménot, G., Combourieu-Nebout, N., Dugerdil, L., Blache, M., Robles, M., Florenzano, A., Masi, A., Mercuri, A. M., Sadori, L., Balasse, M., and Peyron, O.: Holocene climate dynamics in the central Mediterranean inferred from pollen data, Climate of the Past, 21, 2331–2359, https://doi.org/10.5194/cp-21-2331-2025, 2025.

Orbigny, A.: Foraminifères, in de la Sagra, Bertrand, 1–224 pp., 1839.

Ozenda, P.: Végétation du continent européen, Delachaux et Niestlé., 272 pp., 1994.

Paquet, H., Coudé-Gaussen, G., and Rognon, P.: Etude minéralogique de poussière sahariennes le long d'un transect entre 19 et 35° de latitude Nord, Revue de Geographie Physique et de Geologie Dynamique, 25, 257–265, 1984.

https://doi.org/10.5194/egusphere-2026-1342
Preprint. Discussion started: 18 March 2026

834 Peel, M. C., Finlayson, B. L., and McMahon, T. A.: Updated world map of the Köppen-Geiger climate
835 classification, Hydrol. Earth Syst. Sci., 11, 1633–1644, 2007.
836 Peretto, C.: The first peopling of southern Europe: the Italian case, Comptes Rendus Palevol, 5, 283–290,
837 https://doi.org/10.1016/j.crpv.2005.11.006, 2006.
838 Pérez-Folgado, M., Sierro, F. J., Flores, J. A., Cacho, I., Grimalt, J. O., Zahn, R., and Shackleton, N.: Western
839 Mediterranean planktonic foraminifera events and millennial climatic variability during the last 70 kyr, Marine
840 Micropaleontology, 48, 49–70, https://doi.org/10.1016/S0377-8398(02)00160-3, 2003.
841 Petschick, R.: MacDiff Ver.4.2.5, Manual, 2000.
842 Petschick, R., Kuhn, G., and Gingele, F.: Clay mineral distribution in surface sediments of the South Atlantic:
843 sources, transport, and relation to oceanography, Marine Geology, 130, 203–229, https://doi.org/10.1016/0025-
844 3227(95)00148-4, 1996.
845 Peyron, O., Guiot, J., Cheddadi, R., Tarasov, P., Reille, M., De Beaulieu, J.-L., Bottema, S., and Andrieu, V.:
846 Climatic Reconstruction in Europe for 18,000 YR B.P. from Pollen Data, Quat. res., 49, 183–196,
847 https://doi.org/10.1006/qres.1997.1961, 1998.
848 Peyron, O., Goring, S., Dormoy, I., Kotthoff, U., Pross, J., De Beaulieu, J.-L., Drescher-Schneider, R., Vannière,
849 B., and Magny, M.: Holocene seasonality changes in the central Mediterranean region reconstructed from the
850 pollen sequences of Lake Accesa (Italy) and Tenaghi Philippon (Greece), The Holocene, 21, 131–146,
851 https://doi.org/10.1177/0959683610384162, 2011.
852 Peyron, O., Magny, M., Goring, S., Joannin, S., de Beaulieu, J. L., Brugiapaglia, E., Sadori, L., Garfi, G., Kouli,
853 K., Ioakim, C., and Combourieu-Nebout, N.: Contrasting patterns of climatic changes during the Holocene across
854 the Italian Peninsula reconstructed from pollen data, Clim. Past, 2013.
855 Pierce, J. W. and Stanley, D. J.: Suspended-sediment concentration and mineralogy in the central and western
856 Mediterranean and mineralogic comparison with bottom sediment, Marine Geology, 19, M15–M25,
857 https://doi.org/10.1016/0025-3227(75)90053-5, 1975.
858 Pisias, N. G. and Moore, T. C.: The evolution of Pleistocene climate: A time series approach, Earth and Planetary
859 Science Letters, 52, 450–458, https://doi.org/10.1016/0012-821X(81)90197-7, 1981.
860 Prasad, A. M., Iverson, L. R., and Liaw, A.: Newer Classification and Regression Tree Techniques: Bagging and
861 Random Forests for Ecological Prediction, Ecosystems, 9, 181–199, https://doi.org/10.1007/s10021-005-0054-1,
862 2006.
863 Pross, J., Koutsodendris, A., Christanis, K., Fischer, T., Fletcher, W. J., Hardiman, M., Kalaitzidis, S., Knipping,
864 M., Kotthoff, U., Milner, A. M., Müller, U. C., Schmiedl, G., Siavalas, G., Tzedakis, P. C., and Wulf, S.: The 1.35-
865 Ma-long terrestrial climate archive of Tenaghi Philippon, northeastern Greece: Evolution, exploration, and
866 perspectives for future research, nos, 48, 253–276, https://doi.org/10.1127/nos/2015/0063, 2015.
867 Quézel, P. and Médail, F.: Écologie et biogéographie des forêts du bassins méditerranéen, Elsevier., Paris, 571
868 pp., 2003.
869 Robles, M., Peyron, O., Ménot, G., Brugiapaglia, E., Wulf, S., Appelt, O., Blache, M., Vannière, B., Dugerdil, L.,
870 Paura, B., Ansanay-Alex, S., Cromartie, A., Charlet, L., Guédron, S., De Beaulieu, J.-L., and Joannin, S.: Climate
871 changes during the Late Glacial in southern Europe: new insights based on pollen and brGDGTs of Lake Matese
872 in Italy, Clim. Past, 19, 493–515, https://doi.org/10.5194/cp-19-493-2023, 2023.

https://doi.org/10.5194/egusphere-2026-1342
Preprint. Discussion started: 18 March 2026

Robles, M., Andrieu, V., Rochette, P., Fauquette, S., Peyron, O., Demory, F., Parlak, O., Charrat, E., Gambin, B., and Alçiçek, M. C.: Vegetation and climate changes at the Early-Late Pliocene Transition around the Mediterranean basin: A case from the Burdur Basin in Southwestern Anatolia, Climate of the Past, 1–33, https://doi.org/10.5194/egusphere-2025-174, 2025.

Saarinen, J., Oksanen, O., Žliobaitė, I., Fortelius, M., DeMiguel, D., Azanza, B., Bocherens, H., Luzón, C., Solano-García, J., Yravedra, J., Courtenay, L. A., Blain, H.-A., Sánchez-Bandera, C., Serrano-Ramos, A., Rodriguez-Alba, J. J., Viranta, S., Barsky, D., Tallavaara, M., Oms, O., Agustí, J., Ochando, J., Carrión, J. S., and Jiménez-Arenas, J. M.: Pliocene to Middle Pleistocene climate history in the Guadix-Baza Basin, and the environmental conditions of early Homo dispersal in Europe, Quaternary Science Reviews, 268, 107132, https://doi.org/10.1016/j.quascirev.2021.107132, 2021.

Salonen, J. S., Korpela, M., Williams, J. W., and Luoto, M.: Machine-learning based reconstructions of primary and secondary climate variables from North American and European fossil pollen data, Sci Rep, 9, 15805, https://doi.org/10.1038/s41598-019-52293-4, 2019.

Sánchez Goñi, M. F., Llave, E., Oliveira, D., Naughton, F., Desprat, S., Ducassou, E., Hodell, D. A., and Hernández-Molina, F. J.: Climate changes in south western Iberia and Mediterranean Outflow variations during two contrasting cycles of the last 1Myrs: MIS 31–MIS 30 and MIS 12–MIS 11, Global and Planetary Change, 136, 18–29, https://doi.org/10.1016/j.gloplacha.2015.11.006, 2016.

Sánchez-Bandera, C., Fagoaga, A., Serrano-Ramos, A., Solano-García, J., Barsky, D., DeMiguel, D., Ochando, J., Saarinen, J., Piñero, P., Lozano-Fernández, I., Courtenay, L. A., Titton, S., Luzón, C., Bocherens, H., Yravedra, J., Fortelius, M., Agustí, J., Carrión, J. S., Oms, O., Blain, H.-A., and Jiménez-Arenas, J. M.: Glacial/interglacial climate variability in southern Spain during the late Early Pleistocene and climate backdrop for early *Homo* in Europe, Palaeogeography, Palaeoclimatology, Palaeoecology, 625, 16, https://doi.org/10.1016/j.palaeo.2023.111688, 2023.

Sánchez-Garrido, J. C. and Nadal, I.: The Alboran Sea circulation and its biological response: A review, Front. Mar. Sci., 9, 933390, https://doi.org/10.3389/fmars.2022.933390, 2022.

Sánchez-Laulhé, J. M., Jansa, A., and Jiménez, C.: Alboran Sea Area Climate and Weather, in: Alboran Sea - Ecosystems and Marine Resources, edited by: Báez, J. C., Vásquez, J.-T., Camiñas, J. A., and Malouli Idrissi, M., 939, 2021.

Sassoon, D., Combourieu-Nebout, N., Peyron, O., Bertini, A., Toti, F., Lebreton, V., and Moncel, M.-H.: Pollen-based climatic reconstructions for the interglacial analogues of MIS 1 (MIS 19, 11, and 5) in the southwestern Mediterranean: insights from ODP Site 976, Climate of the Past, 21, 489–515, https://doi.org/10.5194/cp-21-489-2025, 2025.

Schiebel, R. and Hemleben, C.: Planktic Foraminifers in the Modern Ocean, Springer Berlin Heidelberg, Berlin, Heidelberg, https://doi.org/10.1007/978-3-662-50297-6, 2017.

Siccha, M. and Kucera, M.: ForCenS, a curated database of planktonic foraminifera census counts in marine surface sediment samples, Sci Data, 4, 170109, https://doi.org/10.1038/sdata.2017.109, 2017.

Skonieczny, C., Bory, A., Bout-Roumazeilles, V., Abouchami, W., Galer, S. J. G., Crosta, X., Stuut, J.-B., Meyer, I., Chiapello, I., Podvin, T., Chatenet, B., Diallo, A., and Ndiaye, T.: The 7–13 March 2006 major Saharan outbreak: Multiproxy characterization of mineral dust deposited on the West African margin, Journal of Geophysical Research: Atmospheres, 116, https://doi.org/10.1029/2011JD016173, 2011.

https://doi.org/10.5194/egusphere-2026-1342
Preprint. Discussion started: 18 March 2026

Stumpf, R., Frank, M., Schönfeld, J., and Haley, B. A.: Climatically driven changes in sediment supply on the SW Iberian shelf since the Last Glacial Maximum, Earth and Planetary Science Letters, 312, 80–90, https://doi.org/10.1016/j.epsl.2011.10.002, 2011.

Tarasov, P. E., Cheddadi, R., Guiot, J., Bottema, S., Peyron, O., Belmonte, J., Ruiz-Sanchez, V., Saadi, F., and Brewer, S.: A method to determine warm and cool steppe biomes from pollen data; application to the Mediterranean and Kazakhstan regions, J. Quaternary Sci., 13, 335–344, https://doi.org/10.1002/(SICI)1099-1417(199807/08)13:4%253C335::AID-JQS375%253E3.0.CO;2-A, 1998.

Ter Braak, C. J. F., Juggins, S., Birks, H. J. B., and Van der Voet, H.: Weighted Averaging Partial Least Squares regression (WA-PLS): definition and comparison with other methods for species-environment calibration, in: Multivariate Environmental Statistics, edited by: Patil, G. P. and Rao, C. R., Amsterdam, 525–560, 1993.

Theron, R., Paillard, D., Cortijo, E., Flores, J. A., Vaquero, M., Sierro, F. J., and Waelbroeck, C.: Data-mining the past environment, in: IGARSS 2003. 2003 IEEE International Geoscience and Remote Sensing Symposium. Proceedings (IEEE Cat. No.03CH37477), IGARSS 2003. 2003 IEEE International Geoscience and Remote Sensing Symposium., 3688–3690, https://doi.org/10.1109/IGARSS.2003.1295238, 2003.

Tintore, J., Violette, P. E. L., Blade, I., and Cruzado, A.: A Study of an Intense Density Front in the Eastern Alboran Sea: The Almeria–Oran Front, Journal of Physical Oceanography, 18, 1384–1397, https://doi.org/10.1175/1520-0485(1988)018%253C1384:ASOAID%253E2.0.CO;2, 1988.

Toti, F., Bertini, A., Girone, A., Marino, M., Maiorano, P., Bassinot, F., Combourieu-Nebout, N., Nomade, S., and Buccianti, A.: Marine and terrestrial climate variability in the western Mediterranean Sea during marine isotope stages 20 and 19, Quaternary Science Reviews, 243, 106486, https://doi.org/10.1016/j.quascirev.2020.106486, 2020.

Voelker, A. H. L., Salgueiro, E., Rodrigues, T., Jimenez-Espejo, F. J., Bahr, A., Alberto, A., Loureiro, I., Padilha, M., Rebotim, A., and Röhl, U.: Mediterranean Outflow and surface water variability off southern Portugal during the early Pleistocene: A snapshot at Marine Isotope Stages 29 to 34 (1020–1135ka), Global and Planetary Change, 133, 223–237, https://doi.org/10.1016/j.gloplacha.2015.08.015, 2015.

Zhao, Y., Liu, Z., Colin, C., Paterne, M., Siani, G., Cheng, X., Duchamp-Alphonse, S., and Xie, X.: Variations of the Nile suspended discharges during the last 1.75Myr, Palaeogeography, Palaeoclimatology, Palaeoecology, 311, 230–241, https://doi.org/10.1016/j.palaeo.2011.09.001, 2011.

Zhao, Y., Colin, C., Liu, Z., Paterne, M., Siani, G., and Xie, X.: Reconstructing precipitation changes in northeastern Africa during the Quaternary by clay mineralogical and geochemical investigations of Nile deep-sea fan sediments, Quaternary Science Reviews, 57, 58–70, https://doi.org/10.1016/j.quascirev.2012.10.009, 2012.

Zhao, Y., Colin, C., Liu, Z., Bonneau, L., and Siani, G.: Climate forcing of terrigenous sediment input to the central Mediterranean Sea since the early Pleistocene, Palaeogeography, Palaeoclimatology, Palaeoecology, 442, 23–35, https://doi.org/10.1016/j.palaeo.2015.11.006, 2016.